MECHANICAL AND ELECTRONIC PROPERTIES OF CUBIC BORON NITRIDE AND CARBON BORON NITRIDE: A QUANTUM MONTE CARLO STUDY

BY

ATAMBO, MICHAEL ONTITA

Reg: SC/PGP/058/11

THESIS SUBMITTED IN PARTIAL FULFILLMENT OF THE REQUIREMENTS FOR THE AWARD OF THE DEGREE OF MASTER OF SCIENCE IN PHYSICS, TO THE SCHOOL OF SCIENCE, UNIVERSITY OF ELDORET, ELDORET.

2013

DECLARATION

Declaration by the student:

I declare that this is my original work and it has never been submitted in any other University or college for examinations or otherwise. No part of this thesis may be reproduced without prior written permission of the author and/or University

Atambo , Michael Ontita

Signature .....Date .....

Reg: SC/PGP/058/11

Declaration by the supervisors:

This thesis has been submitted for examination with our approval as University Supervisors.

Signature: .....Date: .....

Prof. George. O. AMOLO

Department of Physics, University Of Eldoret.

Signature: ..... Date .....

Dr. Nicholas .W. MAKAU

Department of Physics, University Of Eldoret.

DEDICATION

This work is dedicated to my loving and dedicated family.

ABSTRACT

Carbon Boron Nitride (BC_2N) has attracted a lot of attention in research and industry since it was first synthesized and continues to maintain this interest due to the fascinating mechanical and electronic properties that it is proposed to possess. Using First-principles pseudo-potential method and plane-wave methods in Density Functional Theory as well as Quantum Monte Carlo techniques, the mechanical stability and lattice constants of BC_2N have been studied. Cubic BN (c-BN) which is a compound that closely resembles BC_2N in structure, has also been studied comparatively. The lattice parameter for c-BN was found to be 3.6136 Å using Quantum Monte Carlo (QMC) techniques while Density Functional theory (DFT) gave a value of 3.6316 Å. The bulk modulus of c-BN was found to be 365 GPa (DFT) and 393 GPa using QMC, while, the bulk modulus for BC_2N was found to be 365 GPa (DFT) and 395 GPa (QMC), and the calculated lattice parameter 3.63 Å (DFT) and 3.61 Å (QMC). The stability of BC_2N was also investigated using phonon density of states, the phonon dispersion curves, the specific heat, vibrational frequency and internal energy. The same was also done for c-BN for comparison purposes. These thermodynamic properties were investigated so as to establish the lattice dynamics of the materials, and this study found no obvious instabilities in the structure of BC_2N or c-BN, up to temperatures of 2500 K. This confirms that BC_2N is a suitable candidate for use in the hard materials industry just like c-BN, and owing to the reduced energy band gap of 2.5 eV, compared to that of c-BN of 4.4 eV, it can also be used as a semiconductor material.

TABLE OF CONTENTS

LIST OF TABLES

LIST OF FIGURES

ACRONYMS

BC_2N Carbon Boron Nitride.

BO Born-Oppenheimer.

c-BN cubic Boron Nitride.

DFT Density Functional Theory.

DMC Diffusion Monte Carlo.

EELS Electron Energy Loss Spectroscopy.

EOS Equation Of State.

GGA Generalized Gradient Approximation.

GPa Giga Pascal.

HA Harmonic Approximation.

LDA Local Density Approximation.

LSDA Local Spin Density Approximation.

MPC Model Periodic Coulomb.

PBE Perdew Burke and Ernzhoff.

QE opEn Source Package for Research in Electronic Structure, Simulation and Optimization.

QHA Quasi Harmonic Approximation.

QMC Quantum Monte Carlo.

VMC Variational Monte Carlo.

GLOSSARY

bond metallicity the level of delocalization of electrons.

Brillouin zone the set of points in k-space that can be reached from the origin without crossing any Bragg plane.

bulk modulus measures a substances resistance to uniform compression. The pressure required to reduce the volume by 1/e.

Ewald energy electrostatic interaction energy for periodic systems.

exchange correlation interaction between electrons.

functional function of a function.

hardness the ability of a material to resist being scratched or indented by another.

hybridization the mixing of chemical bonds into hybrid orbitals suitable for the pairing of electrons to form chemical bonds.

isoelectronic identical electron configuration.

lattice parameter the length along one of the sides of the unit cell.

phonons a quanta of lattice vibration.

pseudo-potentials a replacement of the strong Coulomb potential and core electrons by a weaker effective potential.

shear modulus the resistance to reversible deformation upon shear.

shear strength strength of a material against a load or force along a plane that is parallel to the direction of the force.

superhard A superhard material is a material with a hardness value exceeding 40 GPa (gigapascals) on vickers hardness test , or Bulk modulus greater than 350GPa.

LIST OF SYMBOLS

β Compressibility, the isothermal change in volume with pressure.

$\Theta_s(\vec{r})$ Blip Function.

k_B Boltzmann Constant.

$\mathring{A}$ Angstrom 10^{-10}m.

Θ_D Debye Temperature.

$D(\vec{R})$ Determinant of a Hartree-Fock Orbital.

Z_β electronic charge.

V volume.

H_m Mohs Hardness.

$J(\vec{R})$ Jastrow Function.

Z_m Maximum valence.

Z_α nuclear charge.

sp^3 hybrid orbital from the mixing of one s and three p orbitals.

V_m Molar Volume.

Z_c cationic valence.

ACKNOWLEDGMENT

I acknowledge my supervisors Prof. George O. Amolo and Dr. Nicholas W. Makau, the members of the Computational Material Science Group at University of Eldoret, both past and present, some of whom include Cecil Moro, George Manyali and Kiptiemoi Korir. I acknowledge the Physics Department as well as Eldoret University for facilitating this work. I also acknowledge the National Council of Science and Technology, which has funded some of the computational resources placed at the disposal of the research group. It is always true that no good work is done by one man, but a team effort, in this regard I would like to acknowledge Prof. Ryo Maezono, from the Japan Advanced Institute of Science and Technology, who went to great lengths to aid this work, both by providing much-needed computational resources, as well as a large amount of his time, when required, to help out when we hit challenges, and for this, we are greatly indebted to him, noting that much of this work would not have been possible without his support.

CHAPTER ONE

INTRODUCTION

1.1 Overview

The term hardness was first coined by the [1], back in 1772, and this physical property has been used as one of the fundamental mechanical aspects of materials since that time. It is conventionally defined at a macroscopic level as the ability of a material to resist being scratched or indented by another. While superhard materials are those that have a hardness that exceeds 40 Giga Pascal (GPa) on the Vickers hardness test [2], well-known examples are Diamond (115 GPa) and cubic Boron Nitride (c-BN) (62 GPa). Hardness in a material can range from one-tenths of a Giga Pascal for some ionic substances like 0.2 GPa for NaCl [3], to tens of Giga Pascals for covalently bonded crystals such as SiC with a hardness of 31 GPa [4] and transition metals with metallic bonding like Tungsten Carbide (24 GPa).

There are two classes of hard materials [5], classified based on the cause of the hardness in the material. The first category are intrinsic superhard materials. The hardness in this category is caused by the strong directional and covalent bonds in the crystal structure, and since the bonding is a three-dimensional configuration, it resists compression as well as bending of the bonds. This category includes materials such as diamond, c-BN, Silicon Carbide and others.

The second category are known as extrinsic superhard materials. These materials have a high value of hardness that is caused by the micro-structure that it possesses, rather than the bonding of the atoms. These materials have a micro-structure that hinders creation and movement of dislocations, and as a result the material achieves high hardness. Examples of this would include aggregated carbon nanorods[6] and rhenium diboride [7].

As of the present, all known superhard materials bond in either covalent or polar covalent fashion [2]. Over the last few decades, a lot of work has been done in an effort to characterise the known superhard materials, and novel superhard materials for both practical and scientific purposes. Some of the studies have aimed at designing materials with desirable technological properties while others aimed at understanding the factors that determine hardness at a microscopic level. Super-hard materials play an important role in technological applications as well as in research. These compounds are used for instance in cutting tool-tips in industry [8], as

abrasive coatings [8], and also as protective coatings [9, 10]. In research, these materials are used as tips in high pressure experiment apparatus, among other uses. A significant amount of superhard materials in use currently are based on the two main materials, namely synthetic diamond and cubic boron Nitride (c-BN). These materials are the top two hardest materials in the list of superhard materials, with diamond being the hardest, and c-BN following as noted before.

Diamond is made up of carbon atoms bonded in a tetrahedral structure, with strong, short covalent bonds, which explain the observed hardness and structural integrity of the material (see fig 1.1). Cubic boron Nitride, has a zinc-blende structure just like diamond, with alternating boron and nitrogen atoms, as seen in fig 1.2. Being group III and V elements, the boron and nitrogen atoms create a lattice that is isoelectronic to diamond, and with their crystal ionic radii being close to that of carbon (Table 1.1), the high hardness associated with c-BN is easily explained. The ionic radii was given by [11], separated out according to the coordination number and spin states. In [11] two values of $r_{ion}(O^{-1})$ were used, one being 140 pm and the other being 126 pm. The data was labeled from 140 pm as the ”Effective” ionic radii, and the latter as the ”Crystal” ionic radii.

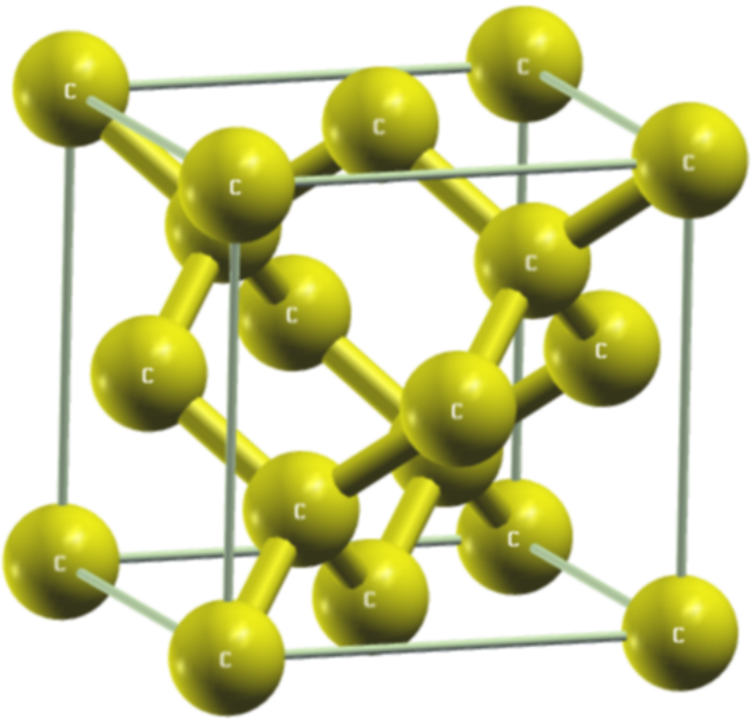

Figure 1.1: Diamond’s atomic structure.

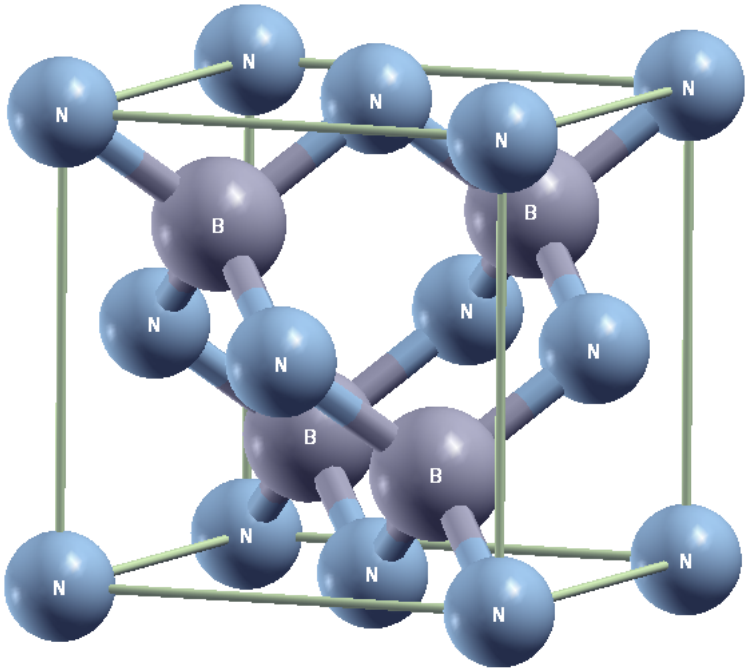

Figure 1.2: Cubic boron Nitride in the Zinc blende structure.

Table 1.1: Ionic radii in Å of B, C and N as a function of ionic charge.

	BN Crystal (Å)		BN Effective (Å)	
Ionic Charge / Element	3+	4+	3+	4+
B	0.41		0.27	
C		0.30		0.16
N	0.30		0.16	

[11]

These two compounds, diamond and c-BN, unfortunately suffer from various setbacks that makes finding their alternatives a worthwhile undertaking. Synthetic diamond, being completely composed of carbon, is not useful in machining ferrous alloys at extreme temperatures and conditions found in industry. This is because carbon dissolves in hot iron, and the machining tool with diamond tips is easily rendered ineffective. This setback has been partly solved by using c-BN in place of diamond, since c-BN does not dissolve in hot iron, and the quality of the tool is thus not adversely affected by hot iron to the same extent.

Though a viable alternative to diamond, c-BN has its own setbacks too , one of which being its low hardness compared to diamond. Cubic BN's hardness is only about half as hard as diamond on the Vickers hardness scale, a fact that makes it disadvantageous to use. This low hardness compared to that of diamond means that in many applications where it is used in place of diamond, the tool life is limited to a significant extent, especially if the materials being worked on by the tool are also hard. Significantly, cost is an important consideration too, since synthetic diamond is actually cheaper to produce than c-BN [12], making the use of c-BN limited by its monetary cost. Thus, the invention and synthesis of novel superhard materials comparable to diamond, is still greatly anticipated.

Currently this impasse is still yet to be satisfactorily dealt with, and researchers are actively looking for solutions. The search for the new superhard material will be guided by these criteria [2]: a three dimensional network structure, strong chemical bonds, short bonds and high charge density. High hardness occurs in the lighter elements of the periodic table, where very short but strong bonds are formed. Diamond satisfies this criteria quite well, and so does boron-based compounds such as c-BN, and other boron rich compounds. These boron rich compounds show desirable properties such as resistance to oxidation, low mass density, high hardness as well as mechanical strength and high wear resistance.

At the moment, a ternary compound named carbon boron Nitride (Carbon Boron Nitride (BC_2N)) is touted as a very likely candidate that can solve the disadvantages associated with diamond and c-BN and is the subject of this study. This compound is expected to demonstrate properties intermediate between those of diamond and those of c-BN. This means the hardness of BC_2N is expected to be higher than that of c-BN while its chemical inertness in the presence of hot ferrous alloys is expected to be better than that of diamond, a situation which indicates

that its an ideal compound with the qualities necessary to fill the gaps left by the disadvantages of c-BN and diamond.

The hardness of BC_2N may be due to the expected short three dimensional covalent bonds, that characterise any superhard material. All the properties of materials are governed by their electronic structure, and it is possible to design materials with certain expected properties, though this is a very demanding task, since the quantitative link between electronic structures and practical macroscopic properties remains a key challenge. Along the same lines is also the theoretical problems that hinder advancement of designer materials. One of this is the lack of a reliable model for the quantification of hardness based on the atomic arrangement. The other challenge is a rigorous definition of hardness at the microscopic level. Both of these challenges will need to be resolved before a clear understanding of hardness and its cause emerges.

Currently two classes of materials show promise in producing materials that can be classified as superhard, these are B-C-N systems (with oxygen in some cases) and the other is formed by light elements like B,C and N bonded to transition metals. This second class is possible only for metals that can induce a high valence electron density onto the corresponding compound, which enables resistance to plastic and elastic deformation. Hardness is physically quantified as the crystal resistance to deformation, and is related to the types of chemical bonds in crystals. For covalent and polar covalent crystals, the bonding is localized in electron pairs, and the hardness is characteristically intrinsic, and is completely dependent on the resistance of the chemical bonds in the crystal within the indentation area, a method used to determine the hardness of materials.

1.2 Binary and Ternary Compounds

1.2.1 Cubic boron Nitride (c-BN)

c-BN was first synthesized in 1957 by [13], and since then it has found numerous applications, as well as being studied by various researchers over the intervening years. Among some of the properties that have intrigued researchers includes its high bulk modulus, large energy band gap and the chemical inertness relative to diamond. The compound does not exist naturally and is synthesized artificially, from hexagonal boron Nitride precursors. The zinc-blende

structure of c-BN was shown previously in the figure 1.2.

1.2.2 Carbon Boron Nitride (BC_2N)

The BC_2N structure selected for this study, is *struc 1* after [14]. This is a zinc blende structure with the ratio of boron to carbon to nitrogen being 1:2:1. The presence of carbon in the structure is expected to play a strengthening role in the crystal. The stronger the bonding in the crystal, the higher the bulk modulus, and consequently the hardness of the material. The expected zinc blende structure is as shown in figure 1.3.

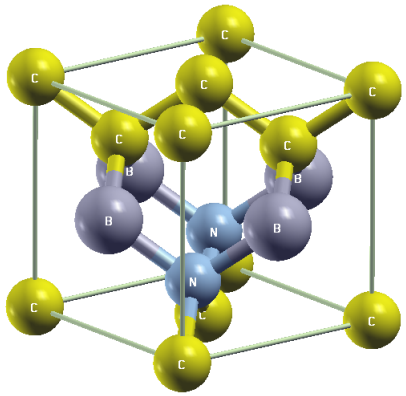

Figure 1.3: The structure of BC_2N.

1.3 Statement of the Problem

The need for advanced materials that serve the requirements of industry and research for superhard compounds is presently high, and work is being done to meet this need. One of the possible candidate materials (BC_2N) has been studied both experimentally [15, 16] and theoretically [17, 18], with these studies indicating that it has high hardness from the values of the bulk modulus (380-400 GPa) and Vickers hardness (76 GPa). However, not all findings about this material are consistent, and some theoretical results have been reported suggesting BC_2N has a lower bulk modulus and hardness than c-BN [19] thereby compounding the problem further.

The present uncertainty in the value of the bulk modulus of BC_2N is a key gap in the industrial applications of the material as well as in scientific research. Determining the true value of the bulk modulus of BC_2N, relative to other superhard materials like c-BN and dia-

mond will not only help in identifying its appropriate applications, but will also aid greatly in the search for superhard materials. The electronic properties of carbon boron nitride have not been investigated systematically, and to better understand the material and its range of potential applications, it is crucial that these properties are studied. Therefore this study is an attempt to accurately predict the value of the bulk modulus, the electronic properties as well as the vibrational and thermodynamic properties of BC_2N and c-BN, using Density Functional Theory and the highly accurate Quantum Monte Carlo technique.

1.4 Significance

Since the situation currently in the search for new superhard materials indicates that the synthesis of new materials with hardness exceeding that of diamond is unlikely, it is more appropriate to search for materials more useful than diamond, as it relates to the total number of applications it can be used for. Owing to the fact that a ternary B-C-N structure may potentially solve the problem of diamond's solubility in iron at high temperatures and also the problem of c-BN's relatively lower hardness compared to diamond, an investigation into such a material is extremely vital at this point in time. In this case, the study of the BC_2N superhard phase is an important step towards ascertaining whether this ternary structure is indeed superhard, and whether it can substitute for c-BN and diamond in the hard materials industry.

1.5 Objectives

1. To obtain the bulk properties of cubic boron Nitride and BC_2N using both Density Functional theory and Quantum Monte Carlo methods.

2. To determine the elastic properties of c-BN and BC_2N.

3. To determine the band structures of the two compounds, c-BN and BC_2N.

4. To investigate the vibrational and thermodynamic properties of c-BN and BC_2N.

CHAPTER TWO

LITERATURE REVIEW

The BC_2N superhard material was synthesised by [15], and it is the publication of this work that attracted a large amount of attention to the compound. However, it is worth noting that there had been a suggestion on its synthesis by [20]. The work of [15] indicated that the compound had a Vickers hardness of 76 GPa, a value that was higher than that of any other known compound apart from diamond. This gave it a greater promise for applications in industry. The bulk modulus reported was a value of 412 ± 9 GPa, a figure that was larger than that of cubic BN, given as 377 GPa in the same work. This high value was noted to be higher than that expected from an ideal mixing of diamond and c-BN.

In a review, [21] reported that full X-ray emission spectra indicated that the stoichiometry of the ternary material B-C-N was BC_2N, while selected area electron diffraction patterns exhibited rings corresponding to the (111),(220) and (311) reflections of the cubic phase. Also noted was the statistically uniform distribution of B,C and N atoms within the crystal lattice, due to the absence of superstructure lines. Electron Energy Loss Spectroscopy (EELS) of the sample also revealed characteristic peaks for sp^3 type bonds, leading to the conclusion of the presence of a diamond like B-C-N phase. However, [15] found that the measured elastic moduli of BC_2N was lower than that of c-BN, but its hardness measured independently by micro and nano-indentation was higher than that of single crystal c-BN.

It study of the ideal strength of the proposed structure was reported in [19], which showed that BC_2N was lower in strength than c-BN. These results were in disagreement with the experimental results of [22] and others [16]. In another work, [17] reported theoretical results that were largely in agreement with [15] work, reporting a bulk modulus for BC_2N of 384 GPa, which was slightly higher than that of c-BN (369 GPa). These recent results supported the earlier theoretical results in [23], which reported a value of 404 GPa for the bulk modulus of BC_2N while placing c-BN at 373 GPa. In [18] the reported theoretical results were qualitatively in agreement with those of [15], noting that the six alloy configurations of BC_2N that they studied demonstrated bulk moduli of 402 GPa, 405 GPa and 383 GPa all of which were higher than that of c-BN, given as 373 GPa in the same work.

It was concluded in [18] that the stability of an alloy configuration was correlated to its density and hardness. Moreover, the higher density configurations coupled with higher bulk moduli as well as higher isotropic shear modulus were more stable. [14] analysed all the feasible 8-atom unit cells of BC_2N. In [14], of the 420 possible configurations, they found that only seven were topologically distinct, and of the seven structures, two demonstrated very high bulk modulus, given as 399 GPa for struc-1 and 400.1 GPa for struc-2 from their designation. At the same time, they found a value of 393 GPa for the bulk modulus of c-BN. Thus, it was concluded that the material synthesized by [16] could be one of these structures. From the available literature, it is clear that there is still some uncertainty as far as the value of the bulk modulus of BC_2N is concerned, as well as the corresponding hardness of c-BN vis a vis BC_2N. This uncertainty goes as far as the structure that should be attributed to the experimental results that demonstrate a high value of BC_2N's hardness and bulk modulus, thus requiring their further investigation.

There is, however, a difference between the bulk modulus of a material, its shear modulus and the hardness (Vickers or otherwise) of a material. However, it has been reported that for materials with a zinc blende (diamond-like) structure, the bulk modulus is one of the best indicators of hardness according to [24]. This is due to the fact that at the microscopic level, it is not just the surface that interacts with the indenter, but the bulk plays a part in the way the material responds to the indenter. Hence, it is for this reason that the bulk properties are critical in studying the hardness of both BC_2N and c-BN. The upper limit of the bulk modulus of a material also serves to indicate the intrinsic compressive hardness of the crystal structure. [24] also found that the bulk modulus increased with decreasing inter atomic distance, average periodic number of constituents, as well as the degree of bond covalence. This phenomena has also been observed in other hard materials made from 4d transition metal Carbides and Nitrides [25]. Moreover, for a compound to satisfy these conditions, it should contain elements located at the top and centre portion of the periodic table. The first period elements do not contain enough electrons to form covalent bonds in three dimensions, therefore, compounds with the highest bulk moduli must be made of elements in the second period i.e. B, C, N.

An illustrative diagram (Fig 2.1) is shown that gives a clear picture of the relationship

between bulk modulus and Vickers hardness, for group IV and group III-V compounds in their cubic form. (Data for Fig. 2.1 after [2, 26, 27, 28]).

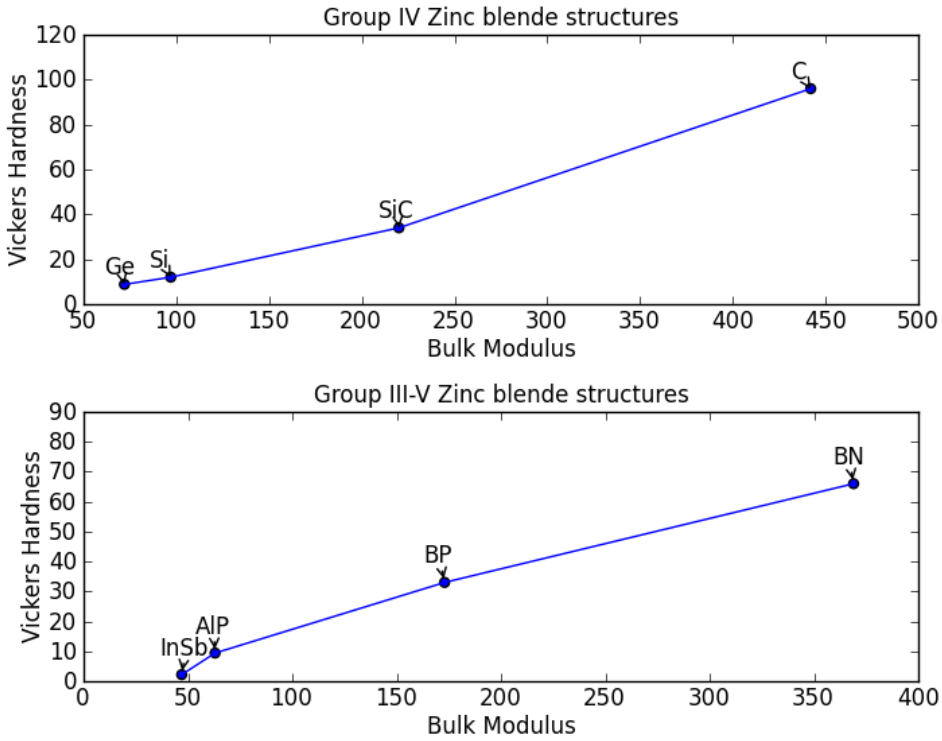

Figure 2.1: Relationship between hardness and Bulk Modulus for specific groups of materials.

CHAPTER THREE

THEORY

3.1 Hardness of Materials

As mentioned earlier, hardness is conventionally defined as the resistance of a material to scratching, or alternatively, could be thought as resistance to plastic deformation such as indention [29, 30]. This physical property is dependent on factors such as the nature of the chemical bond, inter-atomic distances, valence, atomic density and the co-ordination. At present there are several methods in common use to estimate the hardness of materials, among these being the Mohs, Vickers and Knoop tests. Mohs [31] scale, ranks materials in the order of their ability to scratch one another, and numerical values are assigned from 1-10 for certain index-materials. The Vickers [32] test involves measuring the size of an indentation produced by a diamond stylus under a set load. There are other tests used, but they are not as widespread as the ones already mentioned. Those others include are Shore hardness test, polishing hardness, and Brinnell [33] hardness tests.

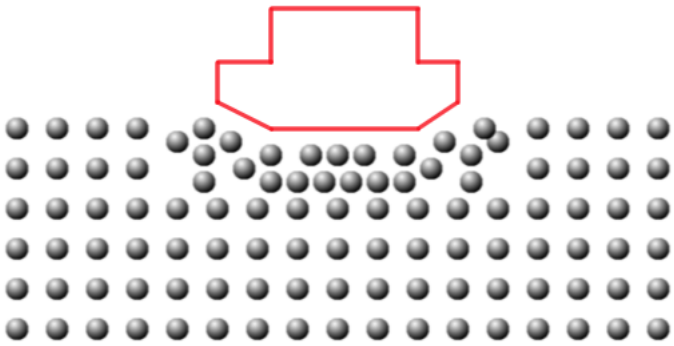

Figure 3.1: An illustration of Hardness testing using a stylus under load.

3.1.1 Compressibility and Bulk Modulus

Compressibility is the isothermal change in volume of a compound with pressure,

$$\beta = -\frac{1}{V}\frac{dV}{dP_T}, \tag{3.1}$$

where the terms in equation 3.1 are the compressibility β, volume V , pressure P and temperature T. The bulk modulus is dependent on the same factors that determine the hardness of a material. This property can be measured directly via change in volume with confining pressure or can be computed from elastic constants. The bulk modulus on the other hand is the reciprocal of the compressibility, $B = \frac{1}{\beta}$, and is more useful in developing predictive models. There are different mathematical models that try to predict hardness of materials using different characteristics of those materials, but from Oganov [34], these models have the following criteria in common:

1. the average bond strength is high,
2. the number of bonds per unit volume is high,
3. the average number of valence electrons per atom is high,
4. bonds are strongly directional.

3.1.2 Relationship Between Hardness and Compressibility

There is an empirical correlation between hardness and compressibility, demonstrated by Beckmann [35], and again by Scott [36] for different minerals. As noted by Goble and Scott [30], the relation between the compressibility and the hardness can be expressed as:

$$H_m = \frac{9}{4}({V_m}^{1/3})(\frac{1}{24}Z_c)^{1/12}B. \tag{3.2}$$

where V_m is the molar volume, B is the bulk modulus, Z_c is the cationic valence and H_m is Mohs hardness. These results from Goble and Scott, show that empirical relationships exist between the bulk modulus (B) and hardness (H_m) for certain groups of minerals. The Mohs hardness is also proportional to the second derivative of lattice energy (U) with change in inter atomic distance r_0, and the absolute hardness can be given by :

$$H = \left(\frac{d^2U}{dr^2}\right)_{r_0}. \tag{3.3}$$

The dependence of the hardness on the atomic separation r_0 rather than on the molar volume V_0 is a reflection of the directional nature of hardness. Thus,

$$\frac{1}{\beta} = \left(\frac{U}{V}\right)\left(\frac{Z_m}{q}\right) = \frac{H}{\frac{Z_m}{q}}. \tag{3.4}$$

In equation 3.4, β is the compressibility and U/V is the volumetric cohesive energy, V is the volume, H is the hardness and Z_m is the maximum valence, m is the number of component atoms, while q is the number of atoms per formula unit. It is worth noting that, in an ideal crystal (without extrinsic impurities), the resistance that a material offers to deformations will be determined by the strength of the local inter-atomic interactions, and for covalent solids, chemical bonds are localized, so that it is not entirely unlikely that compressibility, may be connected to the hardness [37].

3.1.3 Chemical Principles of Hardness

It is known that the strength of a two-centre dual electron chemical bond is largely determined by the overlap of the atomic orbitals of the species involved in the bond. From this we can conclude that the better the overlap between the orbitals, the larger the bond energy as well as the energy gap. Energetically breaking an electron-pair bond inside a crystal means that two electrons become excited from the valence band to the conduction band according to Gilmans assumption [38]. As a result, the resistance force of a bond can be characterized by an energy gap E_g [39]. For covalent crystals the dual-centre, two-electron chemical bonds collectively determine the stabilization factor for the structure and effectively determines the mechanical strength. Strong chemical bonds in a crystal structure will resist isotropic compression as well as shear deformation [2].

3.2 The Many Body Problem and Approximations

The properties of any material may be obtained by solving the wave equation governing the system's dynamics, and for non-relativistic systems, this equation is the Schrödinger equation [40]. This is true in principle, but in practice, the task of solving the equation is an immensely difficult one. The equations that have been solved are for a few simple systems, hence the motivation to use approximations that make the practical calculations possible without sacrificing too much accuracy.

3.2.1 Born-Oppenheimer Approximation

The electric charge on both nuclei and electrons leads to forces of the same order of magnitude, and any change in the momenta of the particles as a result of these forces will also be the same. Assuming the momenta of the electrons and nuclei to be of similar magnitude, and considering the fact that nuclei are so much more massive than the electrons, the nuclei's velocity must therefore be much smaller than that of the electrons [41]. This means that on the time-scale of nuclear-motion, the electrons relax to the instantaneous ground-state configuration, and thus when solving the time-independent Schrödinger equation, Hamiltonian for electrons and nuclei becomes (in atomic units),

$$\begin{aligned} H = \quad & -\tfrac{1}{2}\sum_i \nabla_i^2 - \sum_i \sum_\alpha \tfrac{1}{2m_\alpha} \nabla_\alpha^2 - \sum_i \sum_\alpha \tfrac{Z_\alpha}{|\vec{r_i} - \vec{r_\alpha}|} + \\ & \tfrac{1}{2}\sum_i \sum_{j \neq i} \tfrac{1}{|\vec{r_i} - \vec{r_j}|} + \tfrac{1}{2}\sum_\alpha \sum_{\beta \neq \alpha} \tfrac{Z_\alpha Z_\beta}{|\vec{r_i} - \vec{r_j}|}, \end{aligned} \tag{3.5}$$

where the first term on the right gives the electron kinetic energy, the second term gives the nuclei kinetic energy, the third term gives the electron-nuclear interaction energy, the fourth term the electron-electron interaction energy and the last term is the nuclear-nuclear interaction term. Within the Born-Oppenheimer approximation, we can assume that each nucleus is stationary, and then solve for the ground state of the electronic system. From this, the energy of the system can be obtained and finally one can solve for the nuclear motion.

3.2.2 Hartree Approximation

Here, the wave function is a product *ansatz* of the form :

$$\Psi(\vec{r_1}, \vec{r_2}, \ldots, \vec{r_N}) = \psi_1(\vec{r_1})\psi_2(\vec{r_2}) \ldots \psi_N(\vec{r_N}), \tag{3.6}$$

where this is known as the independent-particle or Hartree approximation [42]. The wave function of the system is made up of a product of orthonormal molecular orbitals. In this case, the electrons only interact with a mean field created by all the other electrons, and instantanous electron-electron interaction is ignored. This approximation is computationally feasible, at

least using self-consistent numerical methods. However, it is a crude approximation that fails to satisfy the Pauli exclusion principle for the many body wave function. Since the Pauli exclusion principle requires the wave function to be antisymmetric with respect to interchange of any two electron coordinates. This condition can not be satisfied by a non-trivial wave-function of the form given by equation 3.6.

3.2.3 Hartree-Fock Approximation

The Hartre-Fock [43] method attempts to correct the failings of the Hartree approximations. It does this by writing the wave function as an anti-symmetrised product of orbitals as in equation 3.7.

$$\Psi(\vec{r}_1,\vec{r}_2,\ldots,\vec{r}_N) = \frac{1}{\sqrt{N}}\mathscr{A}|\psi(\vec{r}_1),\psi(\vec{r}_2)...,\psi(\vec{r}_N)|. \tag{3.7}$$

Slater later realized that the Hartree-Fock wave-function can be efficiently represented by a $N \times N$ determinant, now known as the Slater determinant[44], which is given in equation 3.8, i.e,

$$\Psi(\vec{r}_1,\vec{r}_2,\ldots,\vec{r}_N) = \frac{1}{\sqrt{N!}}\begin{vmatrix} \psi_1(\vec{r}_1) & \psi_2(\vec{r}_1) & \cdots & \psi_N(\vec{r}_1) \\ \psi_1(\vec{r}_2) & \psi_2(\vec{r}_2) & \cdots & \psi_N(\vec{r}_2) \\ \vdots & \vdots & & \vdots \\ \psi_1(\vec{r}_N) & \psi_2(\vec{r}_N) & \cdots & \psi_N(\vec{r}_N) \end{vmatrix}. \tag{3.8}$$

The Hartree-Fock energy can be evaluated by taking the expectation value of the Hamiltonian with the Slater determinant in equation 3.8.

$$\begin{aligned} E_{HF} &= \langle\Psi|H|\Psi\rangle\,, \\ &= \sum_i^N \int \psi^*(\vec{r})\left(-\frac{1}{2}\nabla^2 + v_{ext}(\vec{r})\right)\psi_i(\vec{r})d\vec{r} \\ &\quad + \frac{1}{2}\sum_i^N\sum_j^N \int\int \frac{|\psi_i(\vec{r})|^2|\psi_j(\vec{r})|^2}{|\vec{r}-\vec{r'}|}d\vec{r}d\vec{r'} \\ &\quad - \frac{1}{2}\sum_i^N\sum_j^N \int\int \frac{\psi_i^*(\vec{r})\psi_i(\vec{r'})\psi_j^*(\vec{r'})\psi_j(\vec{r})}{|\vec{r}-\vec{r'}|}\delta_{s_i s_j}d\vec{r}d\vec{r'}, \end{aligned} \tag{3.9}$$

where v_{ext} is the electron-ion potential. The first term in brackets is the kinetic energy summed up with the electron-ion potential, the second term is the Hartree term, which represents the

electrostatic potential. The last term in equation 3.9 is of significant interest since it arises from the antisymmetric nature of the Hartree-Fock wave-function, and it is known as the exchange energy E_X. However, the single-determinant form of the wave-function neglects correlation between electrons, leading to a poor description of the electronic structure of materials since electrons are subjected to an average field created by other electrons that is also non-local.

3.2.4 Post Hartree-Fock Techniques

There are two broad categories of techniques that attempt to solve the limitations of Hartree-Fock; those based on the variational principle and those based on the perturbation technique. Among these are the Configuration interaction [45] and Coupled cluster [46] methods.

3.3 Density Functional Theory (DFT)

This theory was developed by Kohn and Sham in 1965 [47], and it has been extended and used to describe the fundamental properties of materials over the years with a good level of accuracy and computational efficiency. The theory rests on two theorems published in the mid 1960's. The first theorem stated in simple terms that the ground state electron density determines, and uniquely so, all properties of an interacting system of particles from the energy to the wave function. This is significant since the problem of describing systems of particles moves from being a problem of 3N dimensions, with N being the number of particles to a problem of only three spatial variables.

The second theorem states that the electron density that makes the overall functional of the electron density minimum is the true electron density of the system corresponding to a true solution of Schrödinger's equation. The functional described by the Hohenberg-Kohn theorem [48] can be written in terms of single particle wave functions, which collectively define the electron density $n(\vec{r})$. The energy functional (function of a function) can be written as,

$$E[\{\psi_i\}] = \frac{h^2}{m}\sum_i \int \psi_i^* \nabla^2 \psi_i dr^3 + \int V(\vec{r}) n(\vec{r}) dr^3 + \frac{e^2}{2}\int\int \frac{n(\vec{r})n(\vec{r}')}{|\vec{r}-\vec{r}'|} + E_{ion} + E_{XC}[\{\psi_i\}]. \tag{3.10}$$

The terms on the right hand side of equation 3.10 are: the electron kinetic energy, the electron-nuclei interactions, then the electron-electron interactions and the nuclei-nuclei coulomb interactions (E_{ion}) . The final term lumps together the quantum mechanical effects, and the exact form of this term is still not known for all but the simplest systems, but its existence is however guaranteed by the Hohenberg-Kohn theorem [49].

3.3.1 Kohn-Sham Equations

Assuming that the undefined exchange correlation functional can be expressed in a useful form, the minimum energy solutions of the total energy functional has to be found; a task that is made considerably easier than solving the Schrödinger equation for the wave function. This is due to the formulation of the Kohn-Sham equations, that expresses the problem to be solved in single particle form [49]:

$$\left(\frac{h^2}{2m}\nabla^2 + V(\vec{r}) + V_H(\vec{r}) + V_{XC}(\vec{r})\right)\psi_i(\vec{r}) = \varepsilon_i\psi_i(\vec{r}). \tag{3.11}$$

The solutions that are obtained are single-electron wave functions that depend only on three spatial coordinates as mentioned before, which is a large reduction from the $3N$ variables involved in the full solution to the Schrödinger equation. The three potentials that appear in equation 3.11 are the electron-nuclei interaction potential $V(\vec{r})$, then the Hartree potential $V_H(\vec{r})$, that describes the electron-electron interaction and the exchange-correlation potential V_{XC}. The Hartree potential includes a self-interaction contribution, because the electron that is described by the Kohn-Sham equation is also a part of the effective total electron density. The final term in equation 3.11, V_{XC}, describes the exchange and correlation contributions to the single-electron equations, and the correction to the self-interaction problem is lumped in this term.

3.3.2 Local Density Approximation (LDA)

In material science, it is the nature of the electron density that characterizes chemical bonds. As such, we need to solve the Kohn-Sham equations, but to do this we need the unknown exchange-correlation term. Here, an approximation is made, making use of one of the few simple cases where the exact form of the exchange correlation is known, i.e the uniform

electron gas. Though this approximation fails to capture the variations in the electron density, it is, however, still very useful, and is used in practice, with satisfactory results for many systems [40, 49]. The exchange energy for a uniform electron gas is given by the Dirac formula [50],

$$E_X^{LDA}[\rho] = -C_x \int n^{4/3}(\vec{r})dr, \tag{3.12}$$

$$\text{where: } C_x = \frac{3}{4}\left(\frac{3}{\pi}\right)^{1/3}, \tag{3.13}$$

where n is the electron density and the definition C_x is after [50]. Therefore, Local Density Approximation (LDA) assumes that the local density can be treated as a uniform or slowly varying function. This method has been superseded by the Local Spin Density Approximation, that expresses the density separately for electrons with spin up and those with spin down.

$$E_x^{LSDA}(n(\vec{r})) = -\varepsilon_x \int \left(n_\uparrow^{4/3}(\vec{r}) + n_\downarrow^{4/3}(\vec{r})\right) dr, \tag{3.14}$$

$$\text{where: } \varepsilon_x = 2^{1/3} C_x. \tag{3.15}$$

It is understood that Local Spin Density Approximation (LSDA) is implied whenever modern calculations refer to the LDA approximation scheme [50]. This method has been used by physicists and chemists to study periodic (extended) systems such as metals where the approximation of a slowly varying electron density is valid, with accuracy similar to that found in the Hartree-Fock methods. For molecular systems, however, this is not very accurate, and LSDA underestimates the exchange energy quite severely and can create errors that are larger than the whole correlation energy.

3.3.3 Generalized Gradient Approximation (GGA)

The LSDA method is improved upon by considering the non-uniform electron gas [51]. This approach includes information about the density of electrons, as well as the local gradient of this density. There are numerous ways to include the gradient of the density, and this has led to a number of different functionals, the most common of which are the Perdew-Wang (PW91) [52] and Perdew Burke and Ernzhoff (PBE) [53] functionals. For the PBE functional, the

exchange factor is written as an enhancement factor multiplied onto the LSDA functional i.e,

$$\varepsilon_x^{PBE} = \quad \varepsilon_x^{LDA} F(x), \tag{3.16}$$

$$F(x) = \quad 1 + a - \frac{a}{1+bx^2}, \tag{3.17}$$

$$\text{where: } x = \quad \frac{|\nabla n(\vec{r})|}{n(\vec{r})^{4/3}}, \tag{3.18}$$

where the constants a, b are non-empirical parameters. The correlation part is written as an enhancement factor added to the LSDA functional [50].

$$\varepsilon_c^{PBE} = \quad \varepsilon_c^{LDA} + c f_3^3 ln\left[1 + dt^2\left(\frac{1+At^2}{1+At^2+A^2t^4}\right)\right], \tag{3.19}$$

$$\text{where: } A = \quad d\left[exp\left(-\frac{\varepsilon_c^{LDA}}{c f_3^3}\right) - 1\right]^{-1}, \tag{3.20}$$

$$f_3(\zeta) = \quad \frac{1}{2}\left[(1+\zeta)^{2/3} + (1-\zeta)^{2/3}\right], \tag{3.21}$$

$$t = \quad \left[2(3\pi^3)^{1/3} f_3\right]^{-1} x, \tag{3.22}$$

here, ζ is the spin polarization, and c, d are non empirical parameters different from a, b in equation 3.18. The PBE functional has been slightly modified to improve performance for periodic systems, using Revised PBE [54] (revPBE), but at the cost of violating the exchange hole condition (the exchange hole does not sum to -1 as required).

3.3.4 The Quasi Harmonic Approximation

The Debye model of heat capacity in solids is a well established theory in solid state physics. This model explains the low temperature specific heat of solids in terms of the statistical mechanics of an ensemble of harmonic oscillators, or non-interacting particle that are governed by Bose-Einstein statistics. The internal energy of a single oscillator of frequency ω, that is in thermal equilibrium at a temperature T is given by,

$$\bar{E} = \frac{\hbar\omega}{2} + \frac{\hbar\omega}{e^{\frac{\hbar\omega}{k_B T}} - 1}, \tag{3.23}$$

where k_B is the Boltzmann constant. After taking the derivative of the sum over the entire set of possible phonon momenta in the Brillouin zone of equation 3.23 with respect to T, we

arrive at the specific heat at constant volume for a crystal:

$$C_v(T) = \frac{1}{V}\sum_{q\nu} \hbar\omega(\vec{q},\nu)n'(\vec{q},\nu), \tag{3.24}$$

where $\omega(\vec{q},\nu)$ is the frequency of the ν-th phonons mode at a point $\vec{q}$ in the first Brillouin zone. If we then assume that there are three degenerate phonon modes at each point in the Brillouin zone, with each having the frequency $\omega(\vec{q},\nu) = c|\vec{q}|$, where c is the velocity of sound, and then converting the sum in equation 3.24 into an integral, we obtain an expression for the heat capacity. This expression holds in the low temperature limit.

$$C_v(T) = \frac{1}{\Omega}\frac{12\pi^4}{5}k_B\left(\frac{T}{\Theta_D}\right)^3, \tag{3.25}$$

where Ω is the volume of the crystal unit cell and $\Theta_D = \frac{2\pi\hbar}{c}(\frac{2}{4\pi\Omega})^{1/3}$ is the Debye temperature.

In the Born-Oppenheimer approximation, the vibrational properties of molecules and solids are determined by their electronic structure since the ground state energy depends on the coordinates of the atomic nuclei. At low temperatures the amplitudes of the atomic vibrations are much smaller than inter-atomic distances, thus we can assume that the relationship between the ground state energy and the displacement from equilibrium atomic positions is quadratic. This is the Harmonic Approximation (HA), but it suffers from some setbacks such as predicting infinite thermal conductivity, infinite phonon lifetimes, and the independence of vibrational spectra from temperature. The simplest generalization of the HA that corrects to a great extent the mentioned deficiencies is the Quasi Harmonic Approximation (QHA). In QHA, the crystal free energy is assumed to be determined by the vibrational spectrum via the standard harmonic expression,

$$F(X,T) = U_0(X) + \frac{1}{2}\sum_{\vec{r}\nu}\hbar\omega(\vec{q},\nu|X) + k_BT\log\left(1 - e^{-\frac{\hbar\omega(\vec{q},\nu|X)}{k_BT}}\right), \tag{3.26}$$

where X indicates any global static constraint upon which vibrational frequencies may depend, and $U_0(X)$ is the zero temperature energy of the crystal. When $X = V$ (i.e the vibrational frequencies are only constrained by the volume V), differentiation of equation 3.26

with respect to volume lead to the expression for the equation of state,

$$P = -\frac{\partial U_0}{\partial V} + \frac{1}{V}\sum_{\vec{q},\nu} \hbar\omega(\vec{q},\nu)\gamma(\vec{q},\nu)\left(\frac{1}{2} + \frac{1}{e^{\frac{\hbar\omega(\vec{q},\nu|X)}{k_B T}} - 1}\right), \tag{3.27}$$

where,

$$\gamma(\vec{q},\nu) = -\frac{V}{\omega(\vec{q},\nu)}\frac{\partial\omega(\vec{q},\nu)}{\partial V}, \tag{3.28}$$

are the Grüneisen mode parameters. In a perfectly harmonic crystal, phonon frequencies do not depend on the inter-atomic distances, and in such a crystal, equation 3.27 implies that the temperature derivative of pressure at fixed volume vanishes. It follows that the thermal expansivity would also vanish for perfectly harmonic crystals. Following equation 3.24, we can define

$$C_\nu(\vec{q},\nu) = \frac{\hbar\omega(\vec{q},\nu)n'(\vec{q},\nu)}{V}, \tag{3.29}$$

as the contribution of the ν-th normal mode at the $\vec{q}$ point of the Brillouin zone to the total specific heat C_ν, and γ as the weighted average of the various Grüneisen parameters:

$$\gamma = \frac{\sum_{\vec{q}\nu}\gamma(\vec{q},\nu)C_\nu(\vec{q},\nu)}{C_\nu(\vec{q},\nu)}. \tag{3.30}$$

The thermal expansivity in terms of γ is then:

$$\beta = \frac{\gamma C_\nu}{B_T}. \tag{3.31}$$

where B_T is the crystal bulk modulus.

3.3.5 Predictive Computation of *Ab Initio* Phonons

Predictive calculations require a proper quantum-mechanical description of the chemical bonds that hold matter together. This is possible to achieve within electronic structure theory by starting from the Born-Oppenheimer approximation (BO) and using modern developments from Density Functional Theory and perturbation theory [55]. Within the Born-Oppenheimer (BO) approximation, the lattice dynamical properties of a system are determined by the eigen-

values E and eigenfunctions Φ of the schrödinger equation,

$$\left(-\sum_l \frac{\hbar^2}{2M_l}\frac{\partial^2}{\partial \vec{R}^2} + E_{BO}(\vec{R})\right)\Phi(\{\vec{R}_l\}) = E\Phi(\{\vec{R}_l\}), \tag{3.32}$$

where $\vec{R}_l$ is the coordinate of the l-th nucleus, M_l its mass and $\{\vec{R}\}$ indicates the set of all the nuclear coordinates while E_{BO} is the ground state energy of a system of interacting electrons moving in the field of fixed nuclei. The Hamiltonian of this system is,

$$H_{BO}(\{\vec{R}\}) = -\frac{\hbar^2}{2m}\sum_i \frac{\partial^2}{\partial \vec{r}_l{}^2} + \frac{e^2}{2}\sum_{i\neq j}\frac{1}{|\vec{r}_i - \vec{r}_j|} + \sum_i V_{\{\vec{R}\}}(\vec{r}_i) + E_N(\{\vec{R}\}), \tag{3.33}$$

where we have e being the electron charge, $V_{\{\vec{R}\}}$ is the electron-nucleus interaction, and $E_N(\{\vec{R}\}$ is the inter-nuclear interaction energy. The equilibrium geometry is determined by the condition that the forces acting on individual nuclei vanish,

$$\vec{F}_I \equiv -\frac{\partial E_{BO}}{\partial(\{\vec{R}\})} = 0, \tag{3.34}$$

whereas the vibrational frequencies, ω, are determined by the eigenvalues of the Hessian matrix of the BO energy, scaled by the nuclear masses, i.e,

$$det\left|\frac{1}{\sqrt{M_I M_J}}\frac{\partial^2 E_{BO}(\{\vec{R}_I\})}{\partial \vec{R}_I \partial \vec{R}_J} - \omega^2\right| = 0. \tag{3.35}$$

The calculation of the equilibrium geometry and vibrational properties of a system can thus amount to computing the first and second order derivatives of its BO energy surface.

3.4 Quantum Monte Carlo (QMC)

DFT methods are often fast and accurate on many systems. However, DFT has some short comings, one of them being the aforementioned exchange-correlation functional which has to be approximated. This leads to qualitatively wrong answers to some important classes of materials. An alternative is the Quantum Monte Carlo method (QMC) [56] which has some important advantages. It is an explicit many-body method and it also takes care of electron correlation from the start, and is also applicable to finite and periodic systems. QMC

is unbiased in its estimation of the wave-function, since it does not decompose the wave-function into a set of basis functions. The QMC methods encompass three different techniques for treating condensed matter problems; these are Variational Monte Carlo (VMC), Diffusion Monte Carlo (DMC) and Path integral Monte Carlo. A description of VMC and DMC is given in this study, while Path integral Monte Carlo which is used in finite temperature studies is not described, since this work considered only the ground state of the material, with extension to temperature effects being realized using quasi-harmonic approximation (QHA).

3.4.1 Variational Monte Carlo (V.M.C.)

This is a stochastic numerical integration method, capable of computing quantum-mechanical expectation values for any many-body wave-function whose value can be evaluated at arbitrary points in its configuration space. A trial wave function that satisfies some proper boundary conditions, has its total energy calculated as an expectation value of the many-body Hamiltonian operator,

$$< \hat{H} >= \frac{\int E_L(\vec{R})|\Psi(\vec{R})|^2 d\vec{R}}{\int |\Psi(\vec{R})|^2 d\vec{R}}, \tag{3.36}$$

where we have defined the local energy as $E_L(\vec{R}) = \frac{\tilde{H}(\vec{R})\Psi(\vec{R})}{\Psi(\vec{R})}$. The quantity $\vec{R}$ is a $3N$ dimensional vector, which gives the configuration co-ordinates of the N particles in the system. Subsequently the integration is done by sampling at random points in the configuration space of the wave function [57]. From the variational theorem, we know that the energy so obtained in the integration is guaranteed to be an upper limit on the exact ground state energy. There is importance sampling used to sample at groups of points in regions where the integrand is finite, in a way that minimizes the sample variance. This sampling methodology is achieved through the Metropolis scheme, using a modification that employs two-level sampling [57] defined as: First-level acceptance

$$p_1(\vec{R} \leftarrow \vec{R}') = min \left\{ 1, \frac{|D^2_{\uparrow}(\vec{R}) D^2_{\downarrow}(\vec{R})|}{|D^2_{\uparrow}(\vec{R}') D^2_{\downarrow}(\vec{R}')|} \right\}. \tag{3.37}$$

where $p_1(\vec{R} \leftarrow \vec{R}')$ is a probability density function, $\vec{R}$ is a random position where the walker is started, $D(\vec{R})$ is the determinant of a Hartree-Fock orbital and $\vec{R}'$ is a trial position. Second

level acceptance probability:

$$p_1(\vec{R} \leftarrow \vec{R}') = min\left\{1, \frac{exp[2J(\vec{R})]}{2J(\vec{R})]}\right\}. \tag{3.38}$$

where $J(\vec{R})$ is a Jastrow function defined as,

$$J(\vec{R}) = \sum_{i=1}^{N} \chi(r_i) - \frac{1}{2}\sum_{i=1}^{N}\sum_{j=1}^{N} u(\vec{r}_i, \vec{r}_j), \tag{3.39}$$

where χ is a one body, and u a two body correlation term. This two level algorithm has been shown to be more efficient [58] than the standard Metropolis acceptance probability algorithm.

3.4.2 Diffusion Monte Carlo (DMC)

The DMC method is based on rewriting the Schrödinger equation in imaginary time, $\tau = it$, so that it becomes,

$$\frac{\partial |\psi\rangle}{\partial \tau} = \hat{H} |\psi\rangle, \tag{3.40}$$

with the state $|\psi>$ being expanded in eigenstates $|\phi_i>$ of the Hamiltonian, i.e,

$$|\psi\rangle = \sum_{i=0}^{\infty} c_i |\phi_i\rangle. \tag{3.41}$$

A formal solution of the Schrödinger equation then becomes;

$$|\psi(\tau_1 + \delta\tau)\rangle = e^{-\tilde{H}\delta\tau} |\psi(\tau_1)\rangle. \tag{3.42}$$

The state $|\psi>$ evolves from imaginary time τ_1 to a later time $\tau_1 + \delta\tau$. Expanding the initial state in terms of energy ordered eigenstates, one obtains,

$$|\psi(\delta\tau)\rangle = \sum_{i=0}^{\infty} c_i e^{-\varepsilon_i \delta\tau} |\phi_i\rangle. \tag{3.43}$$

Therefore from equation 3.43, any initial state that is not orthogonal to the ground state will

evolve to the ground state ϕ_0 in the long-time limit.

$$\lim_{\tau\to\infty} |\psi(\tau)\rangle = c_o e^{\varepsilon_e \tau} |\phi_o\rangle \,. \tag{3.44}$$

The decay in the exited states in imaginary time evolution is exponentially fast, as opposed to the decay in the VMC method where a contribution remains and adds to the VMC energy. In position space, equation 3.44 becomes,

$$\lim_{\tau\to\infty} \psi(\vec{R},\tau) = c_o e^{\varepsilon_e \tau} \phi_o(\vec{R}). \tag{3.45}$$

The contribution to the VMC energy in equation 3.45 can be kept finite by introducing a constant offset to the energy, $E + T = \varepsilon_o$. If we separate the Hamiltonian into the kinetic energy and the potential energy terms, the imaginary time Schrödinger equation (eqn. 3.40) takes a form similar to a diffusion equation:

$$-\frac{\partial \psi(\vec{R},\tau)}{\partial \tau} = \left[\sum_{i=1}^{N} -\frac{1}{2}\nabla_i^2 \psi(\vec{R},\tau)\right] + (V(\vec{R}) - E_T)\psi(\vec{R},\tau), \tag{3.46}$$

where $\psi(\vec{R},\tau)$ may be understood as being analogous to the density of diffusing particles, while $(V(\vec{R}) - E_T)$ is a rate term describing a potential dependent increase or decrease in the particle density. Equation 3.46 may be understood as a density of particles undergoing diffusion. Figure 3.2 shows an illustration of particle diffusion in imaginary time τ.

As it is, equation 3.46 cannot be implemented efficiently in Monte Carlo Simulations, as the potential $V(\vec{R})$ is unbounded in coulombic systems and hence the rate term $(V(\vec{R}) - E_T)$, can diverge. Large fluctuations in the particle density then result and give impractically large statistical errors. Also, this is missing a key constraint, that is, for fermionic systems, the solution should be antisymmetric with respect to the exchange of any two fermions. The issue of large fluctuations in the particle density can be substantially reduced by the incorporation of importance sampling which is discussed in section 3.4.3. To satisfy the antisymmetry constraint for fermions, a form for the nodal surface of the fermionic wave function is assumed, a method that is referred to as fixed node approximation. Figure 3.3 shows the time evolution of the particle distribution function.

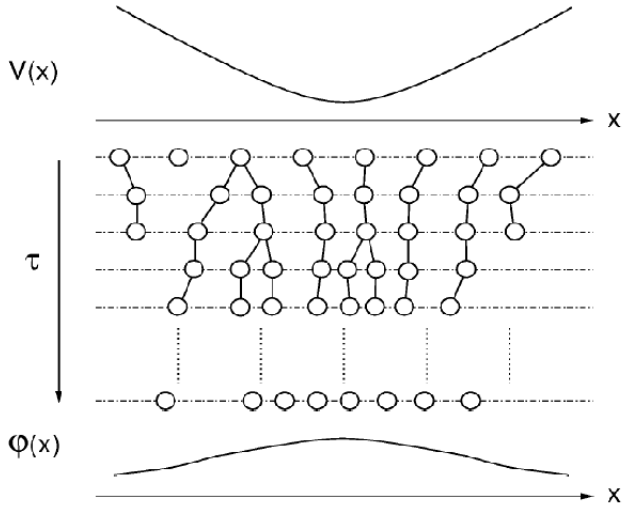

Figure 3.2: Particle diffusion in imaginary time.

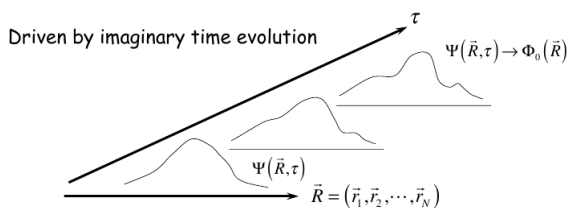

Figure 3.3: The time evolution of the particle distribution function.

3.4.3 Importance Sampling

This is an essential step for the DMC method, for the reason of efficiency. Here, a trial wave function, $\Psi_G(\vec{R})$, closely approximating the ground state wave function is introduced. In this case, we introduce a new distribution,

$$f(\vec{R},\tau) = \phi_G(\vec{R})\phi(\vec{R},\tau), \tag{3.47}$$

where the new term $\phi_G(\vec{R})$ is a guiding wavefunction, and the right side of equation 3.47, happens to be a solution of the Schrödinger equation whenever $\phi(\vec{R},\tau)$ is a solution. Modifying equation 3.46 gives,

$$-\frac{\partial f(\vec{R},\tau)}{\partial \tau} = \left[\sum_{i=1}^{N} -\frac{1}{2}\nabla_i^2 f(\vec{R},\tau)\right] - \nabla\left[\frac{\nabla\psi(\vec{R})}{\psi(\vec{R})} f(\vec{R},\tau)\right] + (E_L(\vec{R}-E_T)f(\vec{R},\tau). \tag{3.48}$$

A trial energy E_T has now been introduced into equation 3.48 to maintain normalization of the projected solution at large τ. The right side of equation 3.48 consists of diffusion, drift and rate terms, respectively. The potential dependent rate term of the non-importance sampled method has been replaced by a term dependent on the difference between the local energy of the guiding wave function and the trial energy. The trial energy is initially chosen to be the VMC energy of the guiding wave function. Using an optimized trial function usually minimizes the difference between the local and trial energies, and consequently the fluctuations in the distribution f are minimized. A wave function optimized using VMC is ideal for this purpose, and is usually the method used in practice to create trial functions.

3.4.4 Fixed Node Approximation

QMC will usually find the minimum energy state, but this state will be a bosonic state, therefore, in order to find the fermionic ground state, an approximation known as the fixed node approximation is made. This makes use of a known trial function to determine the positive and negative regions of the wave function. In this approximation walkers that are attempting to cross the nodes are deleted. The accuracy of this method is therefore dependent on the nodes of the reference wave function.

3.4.5 Localized Basis sets in Quantum Monte Carlo (blip functions)

In QMC calculations, the trial many body wave function $\Psi(\vec{r}_1,\vec{r}_2,\ldots,\vec{r}_N)$ is represented in general by a linear combination of slater determinants D of single electron orbitals $\psi_n(\vec{r}_i)$ multiplied by a parametrised Jastrow correlation factor $J(\vec{r}_1,\vec{r}_2,\ldots,\vec{r}_N)$. Within the VMC method J is optimized by varying its parameters so as to reduce the variance of local energy $\frac{H\Psi_T}{\Psi_T}$, where H is the many body Hamiltonian. The optimised Ψ_T produced by VMC is then passed as input to the DMC calculation, which achieves the exact ground state within the fixed nodal structure required by the Slater determinant D.

At each step of a QMC calculation, it is required that $\Psi(\vec{r}_1,\vec{r}_2,\ldots,\vec{r}_N)$ is evaluated in each walker, involving the evaluation of single electron orbitals, $\psi_n(\vec{r}_i)$. Consequently, the representation of $\psi_n(\vec{r}_i)$ is a crucial issue in the efficiency of the calculations. One of the common approaches is to use Plane-waves, since their accuracy can be systematically improved, they are also unbiased, and most of the readily accessible and technologically developed DFT codes are designed for Plane-wave calculations. However, these plane waves are not well suited for QMC calculations since for the evaluation of each $\psi_n(\vec{r}_i)$, the sum over all the plane-waves in the system has to be found, a process that will lead to very high computational cost. Another option is to use localized basis sets such as gaussians, but these tend to be biased and difficult to systematically improve.

The representation of wave functions in QMC calculations is done more efficiently by using a scheme that is based on B-splines (blip functions) according to [59]. These B-spline functions consist of localized cubic splines centred on the points of a regular grid. This representation is localized, and the evaluation of each orbital $\psi_n(\vec{r}_i)$ has a computational cost that is independent of the system size as well as the blip-grid spacing. B-splines can be obtained from any standard plane-waves density functional theory code, and as such they provide a convenient interface between the plane wave calculations and QMC calculations. These blip functions consist of localized cubic splines centred on a regular grid with each function being non zero inside a region extending two grid spacings in each direction from its center. A blip function $\Theta_s(\vec{r})$ centred on a cubic grid of spacing a, at position $\vec{R}_x = (X_s, Y_c, Z_s)$ is given by:

$$\Theta_s(\vec{r}) = \phi\left(\frac{x-X_s}{a}\right)\left(\frac{y-Y_s}{a}\right)\left(\frac{z-Z_s}{a}\right). \tag{3.49}$$

where $\phi(x)$ is:

$$\begin{aligned}\phi(x) &= 1-\frac{3}{2}x^2+\frac{3}{4}|x|^3, && 0\leq|x|\leq 1,\\ &= \frac{1}{4}(2-|x|)^3, && 1\leq|x|\leq 2,\\ &= 0, && |x|\geq 2\end{aligned} \tag{3.50}$$

Each single particle is then represented as:

$$\psi_n(\vec{r}) = \sum_s a_{ns}\Theta_s(\vec{r}). \tag{3.51}$$

Therefore, for any position $\vec{r}$, there will only be 64 non zero blip functions [59] regardless of the size of the system, meaning that the number of operations required to determine $\psi_n(\vec{r})$ is identical for all materials.

CHAPTER FOUR

METHODOLOGY

4.1 Introduction

This research used two computational approaches in the study of materials, i.e. Quantum Espresso [60] an implementation of Density Functional Theory, and the other is CASINO [61] an implementation of Quantum Monte Carlo methods.

4.2 Electronic and structural Optimization

All calculations involving Density Functional Theory studies were done using the electronic structure code known as Quantum Espresso. This stands for opEn Source Package for Research in Electronic Structure, Simulation and Optimization (QE) and it is a suite of computer codes for first principles materials modelling based on plane waves and pseudo-potentials as well as Density Functional Theory. It is released under a research-friendly (GNU) General Public License [62], and has been developed and tested by the authors [60] as well as many leading research groups around the world for about twenty years. Some of its capabilities include:

1. Calculation of Kohn-Sham orbitals and energies for isolated and periodic systems in their ground-state.

2. Structural optimization of the atomic coordinates and unit cell degrees of freedom using Hellmann-Feynman forces and stresses.

3. Ground state determination of magnetic or spin-polarized systems, including spin-orbit coupling and non-collinear magnetism.

4. *ab initio* molecular dynamics (MD), using either the Car-Parinello Lagrangian, or the Hellmann-Feynman forces.

5. Generation of maximally localized Wannier functions and related quantities.

6. Density-functional perturbation theory, to calculate the second and third derivatives of

the total energy at any arbitrary wavelength, providing phonon dispersions, electron-phonon and phonon-phonon interactions.

Quantum Espresso uses an iterative approach to reach self consistency, which is achieved through the modified Broyden method [63], making use of iterative diagonalization. Norm Conserving [64], Ultra-soft Pseudo Potentials [65, 66], as well as the Projector Augmented wave [67] methods are implemented. There is also an implementation of both the Local density approximation as well as the Generalized gradient approximation exchange-correlation functional. Structural aspects of crystals are treated via the Broyden-Fletcher-Goldfab-Shanno (BFGS) algorithm [68, 69, 70] or the damped dynamics method. These two structural optimizations can be used and they involve the internal microscopic degrees of freedom or the macroscopic degrees of freedom. The second and third order derivatives of the energy with respect to the atomic displacements as well as the electric fields can also be found, with an emphasis on taking advantage of symmetry to reduce the computational cost of the calculations. Electron-phonon interactions can also be determined using this code via a response of the self-consistent potential to a lattice distortion.

4.2.1 The Unit Cell Definition

The structure representing cubic boron Nitride was defined as having a boron atom at (0,0,0) and a nitrogen atom at (0.25,0.25,0.25) with the lattice vectors defined as:

$$\vec{a_1} = a(0.5, 0.5, 0) \qquad \vec{a_2} = a(0, 0.5, 0.5) \qquad \vec{a_3} = a(0.5, 0, 0.5) \tag{4.1}$$

These are simply the primitive vectors of a face centred cubic structure.

For BC_2N the starting unit cell was defined with eight atoms. The ratio of carbon to boron to nitrogen was 2:1:1, and tetrahedral bonding was assumed, with boron and nitrogen bonding with carbon and with each other. The structure of BC_2N used in this study separated the $B-N$ layers from the $C-C$ layers, a configuration that lowers the overall energy of the system and consequently makes the structure more stable [14].

4.2.2 Convergence Testing

The Monkhorst-Pack [71] grid was tested thoroughly from $2\times2\times2$ to $8\times8\times8$, and after careful optimization, a grid of $4\times4\times4$ was used to ensure computational tractability in the ensuing QMC calculations. The plane wave cut-off energy convergence led to a value of 70 Ry for BC_2N and 120 Ry for BN. Convergence was considered to have been achieved when the difference between successive self consistent steps was less than 10^{-6} Ry. The details of the optimization are given in Appendix. A.

4.2.3 Elastic Constants

Elastic constants were calculated from the variation in energy found by applying a small strain to the equilibrium lattice configuration [72, 73]. The energy of a solid under strain is calculated from:

$$\Delta E = \frac{V}{2}\sum_{i=1}^{6}\sum_{j=1}^{6} C_{ij}e_ie_j, \tag{4.2}$$

where V is the volume of the original unstrained lattice, and ΔE is the change in energy caused by a strain with vector $e=(e_1,e_2,e_3,e_4,e_5,e_6)$. C is the matrix of the elastic constants. There are only three independent elastic constants in cubic structures, and they are C_{11}, C_{12} and C_{44}. The primitive lattice vectors for the simple cubic structure are given as:

$$\begin{pmatrix} a_1 \\ a_2 \\ a_3 \end{pmatrix} = \begin{pmatrix} a & 0 & 0 \\ 0 & a & 0 \\ 0 & 0 & a \end{pmatrix}.$$

The primitive vectors $a_i (i=1,\ldots,3)$, were skewed to the strained vectors by the transformation:

$$\begin{pmatrix} a_1' \\ a_2' \\ a_3' \end{pmatrix} = \begin{pmatrix} a_1 \\ a_2 \\ a_3 \end{pmatrix} \cdot (\mathbf{I}+\boldsymbol{\varepsilon}), \tag{4.3}$$

where ε is the strain tensor, related to the strain vector e by:

$$\varepsilon = \begin{pmatrix} e_1 & \frac{e_6}{2} & \frac{e_5}{2} \\ \frac{e_6}{2} & e_2 & \frac{e_4}{2} \\ \frac{e_5}{2} & \frac{e_4}{2} & e_3 \end{pmatrix}. \tag{4.4}$$

The elastic constants for the cubic structures were calculated by applying the tri-axial shear strain $e = (0,0,0,\delta,\delta,\delta)$ to the crystal, and in this case, C_{44} was obtained from:

$$\frac{\Delta E}{V} = \frac{3}{2} C_{44} \delta^2, \tag{4.5}$$

and the shear modulus, $C' = \frac{1}{2}(C_{11} - C_{12})$, was calculated from the orthorhombic strain (volume conserving) $e = (\delta, \delta, (1+\delta)^{-2} - 1, 0, 0, 0)$ using the relation,

$$\frac{\Delta E}{V} = 6C'\delta^2 + O(\delta^3). \tag{4.6}$$

Using equations 4.5 and 4.6, 21 sets of $\frac{\Delta E}{V}$ vs δ values were obtained using DFT calculations by varying δ from -0.02 to 0.02. The data was then fitted to a quadratic polynomial and the corresponding elastic constants were calculated from the coefficient of the quadratic terms in equations 4.5 and 4.6.

4.3 QMC

The CASINO [61] program is an implementation of the Quantum Monte Carlo method, created at Cambridge University Cavendish Laboratory. Its functionality includes the following methods.

1. Variational Monte Carlo (VMC) and,
2. Diffusion Monte Carlo (DMC)

CASINO can also treat the following systems (though not an exhaustive list):

1. Atoms, molecules, polymers, slabs and solids.
2. 1-D, 2-D, and 3-D electron and electron-hole phases with fluid or crystal wave functions, and arbitrary cell shape or spin or polarization density.

Some of the wavefunction representations that it can handle include:

1. Multi-determinant Slater-Jastrow wavefunctions.
2. Orbitals expanded in Gaussian basis set.
3. Orbitals in blip [59] functions.
4. Localized orbitals and basis functions.

In this study the procedure followed in the QMC calculations was as follows:

1. DFT calculations using the optimized unit cell geometry were performed to produce single particle orbital wavefunctions.
2. The obtained single particle wavefunctions were then used to construct the trial wave functions (plane waves) to be used in QMC.
3. The trial wave function was then optimized using VMC, since it provides the upper bound on the ground-state energy using the variational principle applied to the trial form of the many-body wave function, as well as being relatively faster than DMC.
4. A VMC run was then carried out, whereby the total energy E for the ground state was obtained for the various values of lattice constants as was the case in the DFT computations. Energy and volume (E-V) data was also collected, which was then fitted to the Birch-Murnaghan and Vinet equations of state.
5. The optimized VMC wave function was then used as an input wave function for DMC calculations. The DMC calculations were done in three stages,
    (a) VMC Configuration generation;
    (b) DMC equilibration; and
    (c) DMC statistics accumulation.
6. The total energy E for the ground state was then obtained for the various values of lattice constants as was the case in the DFT computations. E-V data was also collected, and that was then fitted to the Birch-Murnaghan and Vinet equations of state, just like in step 5 above.

CHAPTER FIVE

RESULTS AND DISCUSSION

In this chapter, the results obtained in this work are presented. This includes results on the mechanical properties followed by the elastic properties, then the electronic properties and finally the thermal and vibrational properties for both c-BN and BC_2N.

5.1 Mechanical properties for Boron Nitride (c-BN) and Carbon Boron Nitride (BC_2N)

Figures 5.1 and 5.2 show the optimized crystal structures of c-BN and BC_2N, respectively, following a rigorous relaxation procedure. These structures were used as the basis for calculation of the various mechanical, electronic, thermal and vibrational properties of the two compounds. The bond lengths between the atoms in the two structures are shown in Table 5.1. These show that the presence of carbon in the structure influences the bonding significantly, and it is also clearly observed that the C-C bonds are significantly shorter than the C-B, or even the C-N bonds. However the B-N bond in BC_2N is slightly longer (1.58 Å) than that in c-BN (1.55 Å). The length of the two bonds B-N and C-B in BC_2N differ by only 3% from the C-C bonds in diamond which are 1.53 Å. This similarity in bond lengths with those of diamond coupled with similar crystal structures confirms their high hardness relative to that of diamond. The bonding in the two materials is expected to be sp3 hybridization between the 2p orbitals of B and the 2p orbitals of C in BC_2N.

Table 5.1: Calculated DFT-GGA bond lengths in BC_2N and BN.

BC_2N	C-C	1.53 $\mathring{A}$
	B-N	1.58 Å
	C-B	1.58 Å
BN	B-N	1.55 Å

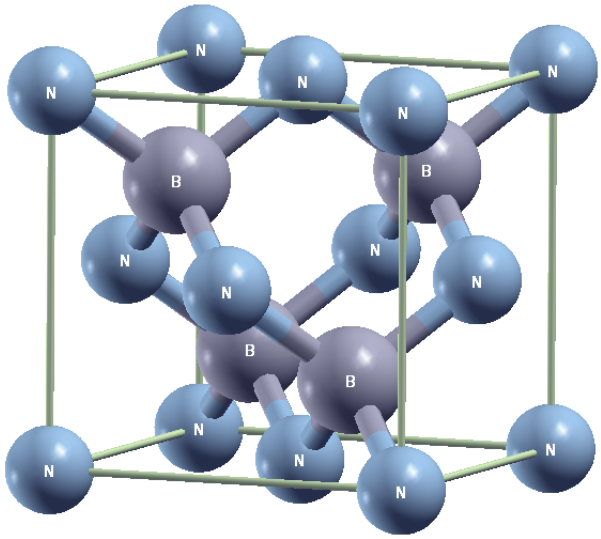

Figure 5.1: Cubic boron Nitride Zinc blende structure.

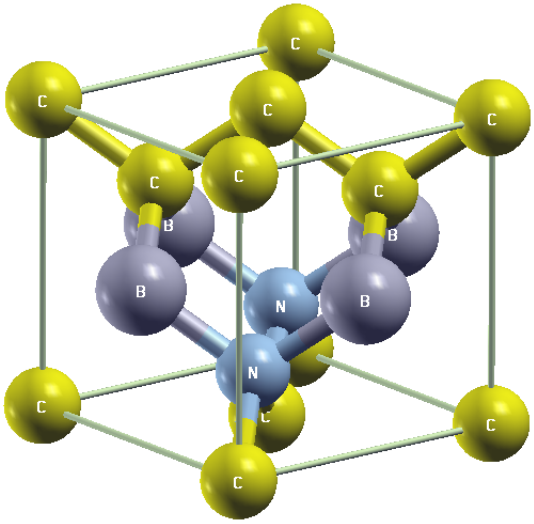

Figure 5.2: BC_2N **Zinc blende structure.**

Other properties of the two materials which include the equilibrium lattice constant are given in Table 5.2, the bulk modulus, unit cell volumes and the pressure derivative of the bulk modulus using DFT in Table 5.3, as well as values from Ewald energy in Table 5.4 and also from Model Periodic Coulomb (MPC) energy vs. volume data as shown in Table 5.5.

Table 5.2 shows the calculated lattice parameter for both c-BN and BC_2N. The results show that DFT tends to overestimate the lattice parameter compared to the experimental value, giving a value of 3.628 Å from the Vinet Equation Of State (EOS), while from DMC, the lattice parameter was obtained at 3.611 Å which was much closer to the experimental value of 3.617 Å for c-BN. Results of the lattice parameter for BC_2N showed that, DFT gave a value of 3.633 Å, while DMC (MPC), gave a value of 3.6127 Å. The DMC (MPC) results are again much closer to the experimental value of 3.602 Å, differing only by 0.53% for the Vinet EOS and 0.55 for the Birch-Murnagan EOS. The observed lattice parameters for both BC_2N and c-BN together with the short bond lengths are the principle determining factors of the high bulk modulus in diamond-like materials [74].

Table 5.2: Calculated Lattice Parameters for BN and BC_2N, using the Vinet and Birch -Murnagan (B-M) equation of state.

BN					
	Vinet EOS (in Å)	B-M EOS (in Å)	Expt. (in Å)	% dev Vinet EOS	%dev B-M EOS
DFT	3.6282	3.6316	3.617[b]	0.56	0.73
Ewald	3.6091	3.6117		0.395	-0.26
MPC	3.6111	3.6136		-0.295	-0.17
BC_2N					
	Vinet EOS (in Å)	B-M EOS (in Å)	Expt (in Å)	% dev Vinet EOS	%dev B-M EOS
DFT	3.6335	3.6343	3.602[b],3.602[c]	1.57	1.65
Ewald	3.6112	3.6116		0.46	0.48
MPC	3.6127	3.6131		0.53	0.55

[b][16] [c][75]

The values of the bulk moduli for both c-BN and BC_2N are shown in Table 5.3, whereby the values predicted by DFT indicates that the hardness of c-BN is lower than that of BC_2N, with their bulk moduli differing by 3.6 GPa. This difference in their bulk moduli is however not very much pronounced, and given that DFT is known to underestimate some properties, it is hard to conclusively pick which material is actually harder between the two, especially basing the judgement on the DFT results alone. BC_2N was found to have a bulk modulus of 369 GPa using the fit to the Birch-Murnagan equation of state while c-BN had a value of 365

Table 5.3: Calculated bulk modulus B_0, and its derivative B'_0 and the unit cell volumes for BN and BC_2N from DFT.

BN			
	B-M EOS	Vinet EOS	Expt.
V_0 $(a.u.^3)$	80.8054	80.5757	
B_0 (GPa)	365.35	364.59	368[b],369[d], 400[e]
B'_{0p}	3.64	3.86	
BC_2N			
	B-M EOS	Vinet EOS	Expt.
V_0 ($a.u.^3$)	323.9292	323.7209	
B_0 GPa	369.02	372.03	355[b],282[c], 412[f]
B'_{0p}	3.61	3.66	

[b][16] [d][76] [e][77] [f][78]

GPa, which was a small difference in the compressibility of the two materials.

A fit to the Vinet equation of state gave values of 365 GPa and 372 GPa for c-BN and BC_2N respectively. Overall, the two approaches i.e Vinet and Birch-Murnaghan, predicted a higher value of bulk modulus for BC_2N compared to that of c-BN.

Table 5.4: B'_0 and the unit cell volumes for BN and BC_2N from Ewald energy. The values in brackets are the error bars, and B-M means Birch-Murnagan equation of state.

BN				BC_2N		
	B-M	Vinet	Exp	B-M	Vinet	Exp
V_0	79.48(3)	79.31(3)		317.9(3)	317.8(4)	
B_0	393(1)	391(1)	368[b],369[d], 400[e]	393(2)	396(2)	355[b],282[c], 412[f]
B'_{0p}	3.602(5)	3.79(1)		3.58(6)	3.60(7)	

[b][16] [d][76] [e][77] [f][78]

The more accurate QMC method, gives a clearer picture of why it is not easy to judge which material between c-BN and BC_2N is actually harder from the calculations alone. So far various experimental results have given inconclusive results on the hardness and bulk modulus of c-BN and BC_2N. From Table 5.4 the closely predicted values of bulk modulus, and its pressure derivative shows that the hardness of BC_2N could be higher than that of c-BN, but the error bars leave a small margin for error on this result. In spite of this, BC_2N is still predicted to have a higher bulk modulus and hence harder than c-BN. The unit cell volume of BC_2N is for the 8 atom cell, and therefore the short inter-atomic distances implies a very high electron density within the material, a situation that is expected for any material to achieve high hardness.

Table 5.5: Calculated B_0, B'_0 and the unit cell volumes for BN and BC_2N from MPC. Error bars are given in brackets.

BN			
	B-M EOS	Vinet EOS	Exp
V_0	79.61(3)	79.44(3)	
B_0	393(1)	391(1)	368[b],369[d], 400[e], 369-400[g]
B'_{0p}	3.599(5)	3.79(1)	
BC_2N			
	B-M EOS	Vinet EOS	Exp
V_0	318.3(3)	318.2(4)	
B_0	395(2)	395(2)	355[b],282[c], 412[f]
B'_{0p}	3.59(7)	3.62(8)	

[b][16] [d][76] [e][77] [f][78] [g][72]

In summary, the results from the Quantum Monte Carlo calculations (given in Tables 5.4 and 5.5) indicate that the bulk modulus of BC_2N is higher than that of c-BN, though their values are close. The fact that bulk modulus is inversely proportional to the compressibility of the material, is an indication that a high bulk modulus suggests high hardness of the material. From theory, the low compressibility is expected to occur whenever there is high valence charge density and strong directional bonds, which ultimately contributes to the resistance to deformation per unit area.

The results obtained in this study are compared with available experimental data, and also other theoretical calculations are shown where available. It is important to note that the bulk modulus, the lattice parameters and the bond lengths reported here are predictions of the ground state and not at finite temperatures. The calculated values for the lattice parameter were found to be in good agreement with the experimental values and other published theoretical works using different techniques. The DMC (MPC) results showed the lowest deviation from the quoted experimental values and hence more accurate. The LDA and GGA results were also found to be close to experimental findings, and are therefore capable of approximating the lattice parameter fairly accurately.

Figure 5.3 shows the Vickers hardness of different compounds plotted against the bulk modulus (after [25, 26], values for c-BN and BC_2N from this work). BC_2N and c-BN occupy the top right hand side of the figure, together with diamond, and all three have in common three dimensional tetrahedral bonds. On the lower right hand side are compounds such as RuB_2 which also has a high bulk modulus (382 GPa) due to the high electronic density that is

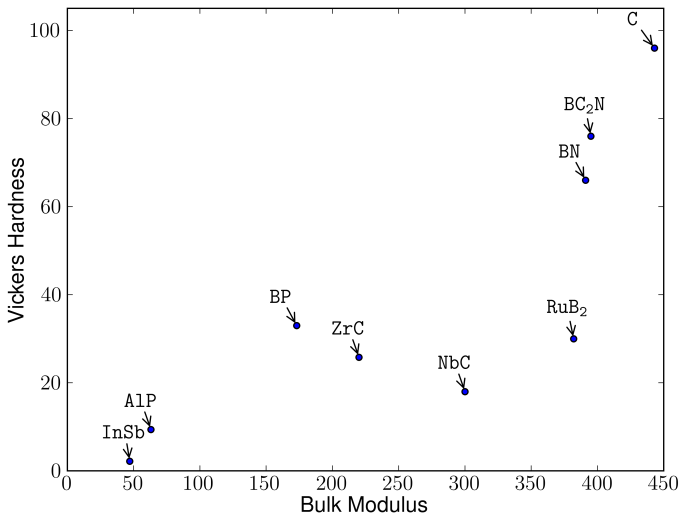

Figure 5.3: A summary and comparison of c-BN, BC_2N and other compounds including Transition metal Carbides and Nitrides.

created by the metal in the compound, but rather low Vickers hardness due to the bond metallicity, a phenomena that makes bending of bonds much easier. Overall, there is a relationship between the Vickers hardness and the bulk modulus, whereby diamond, BC_2N and c-BN are the materials with the highest values of the two and hence hardest.

5.2 Elastic Properties

The elastic properties of c-BN and BC_2N are presented in this subsection. Figures 5.4-5.6 show the plots of $\frac{\Delta E}{V}$ vs distortion, for obtaining the required elastic constants according to equations 4.5 and 4.6. All the plots show the expected quadratic nature as predicated by the respective equations. Table 5.6 shows the calculated average shear moduli C_{44} and C', together with experimental data and other calculated data where available. As noted earlier a high value of elastic constant indicates a harder material and vice versa.

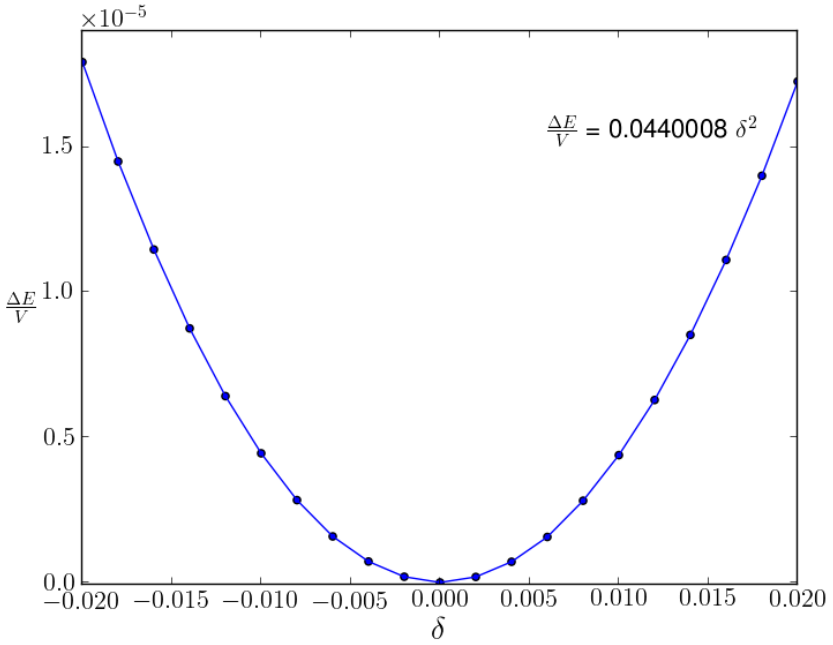

Figure 5.4: Variation of $\frac{\Delta E}{V}$ vs strain δ for the calculation of the C_{44} constant for $c-BN$.

Table 5.6: Calculated Elastic Parameters of BN and BC_2N.

	BN				BC_2N		
	This work	Expt	% dev.	Others	This work	Expt.	Others
C_{44} (GPa)	431	480[a]	10%	471.7[b], 483[d], 493[e]	457		484.2 [b]
C'	317	315[a]	0.63%	310.5[b]	360		352.4 [b]

[a][79] [b][14] [d][80] [e][81]

For c-BN, the value of C_{44} that was calculated had a 10% deviation from published experimental values, while that for C' on the other hand had a deviation of 0.63%. For BC_2N a comparison with other different theoretical results is shown. From the computed results BC_2N was found to have a value of 360 GPa for the shear modulus C', while c-BN had a value of 317 GPa. From the values of the shear modulus (C'), and the constant C_{44}, the shear strength of

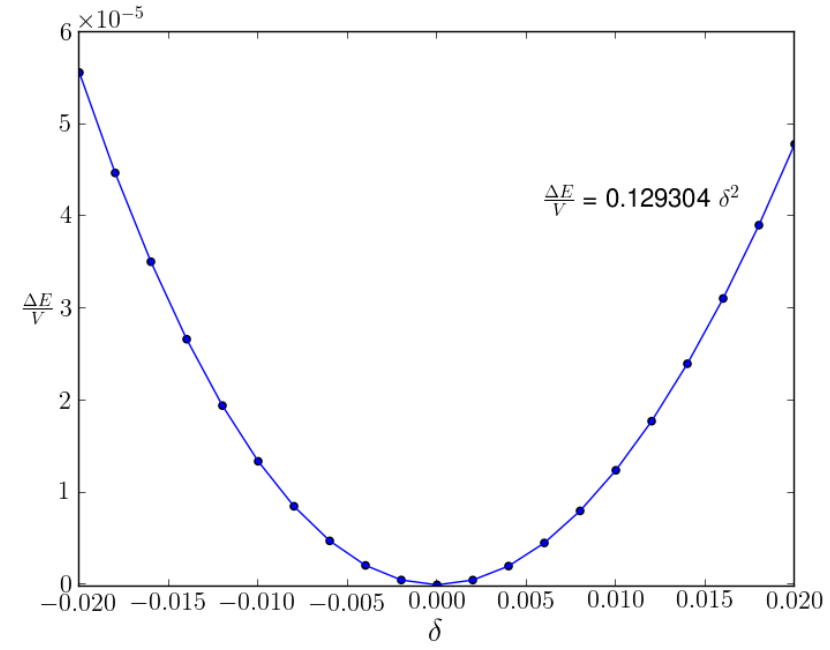

Figure 5.5: Variation of $\frac{\Delta E}{V}$ vs strain δ for the calculation of the C' constant for $c-BN$.

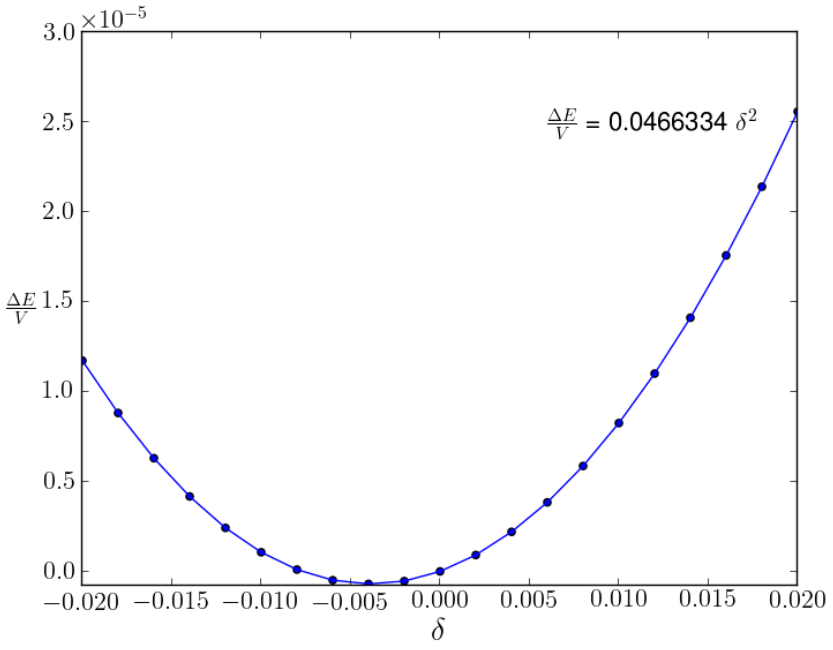

Figure 5.6: Variation of $\frac{\Delta E}{V}$ vs strain δ for the calculation of the C_{44} constant for BC_2N.

BC_2N was predicted to be higher than that of c-BN, results that corroborate the findings from the bulk moduli and the lattice parameters already presented in this work. While the average shear modulus which is given by the C_{44} elastic constant was underestimated by about 10%, the C' elastic constant showed very good agreement with the experimental data, differing by only 0.63%. The underestimation in the shear modulus may be attributed to the limitations in

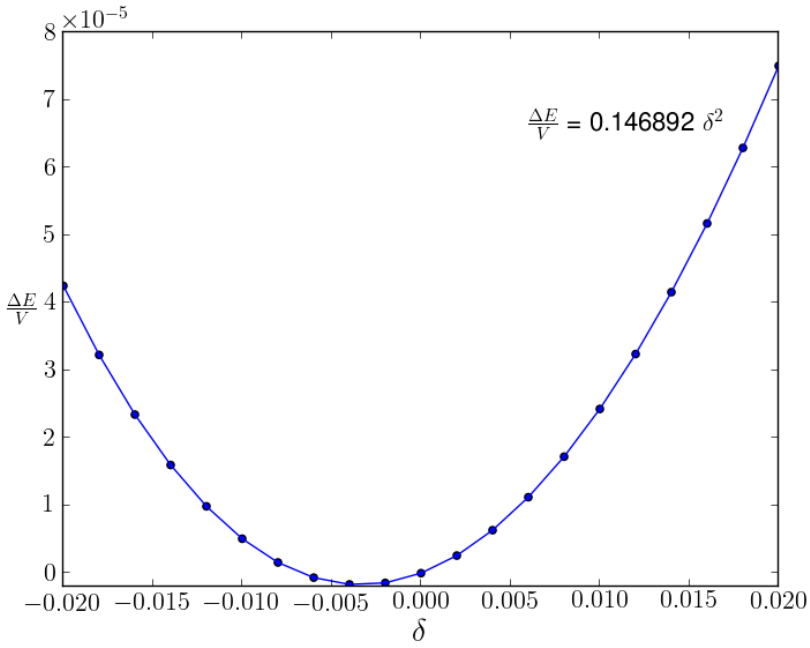

Figure 5.7: Variation of $\frac{\Delta E}{V}$ vs strain δ for the calculation of the C' constant for BC_2N.

the treatment of electron correlation inherent in DFT, due to approximations that are made in practice.

The elastic constants are indicative of the stress required to maintain distortion on a material, and the higher the value of the constant, the more the compressive strength the material possesses.

5.3 Electronic Properties

5.3.1 Band Structure and Density of States

The electronic band structure and density of states for both c-BN and BC_2N are shown in figures 5.8-5.13, while a summary of the energy band gaps of two materials is shown in Table 5.7.

Table 5.7: Calculated Energy Band gaps of c-BN and BC_2N.

	BN	Calc(eV)	Exp.[a]	% Err.	BC_2N	Others[b]
indirect	$\Gamma \rightarrow X$	4.4	5.18	-15 %		
Direct	$\Gamma \rightarrow \Gamma$	8.68	8.0	8.04 %	2.5	2.0
	K→K	11.2	11.8	-5.0 %		

[82][a] [83][b]

Figure 5.8 shows the band structure of c-BN, while figure 5.9 shows the corresponding density of states. An indirect wide band gap of 4.4 eV is clearly seen from Γ to X, since the conduction band minima occurs at X while the valence band maxima is found at Γ. The states located between -20 and -14 eV are mainly the N-2s and B-2s orbitals, while the valence band is dominated by the B-2p and N-2p orbitals. This suggests a strong hybridization of the 2p orbitals of the two elements which may be responsible for the strong bonding seen in c-BN, and hence its reported high bulk modulus.

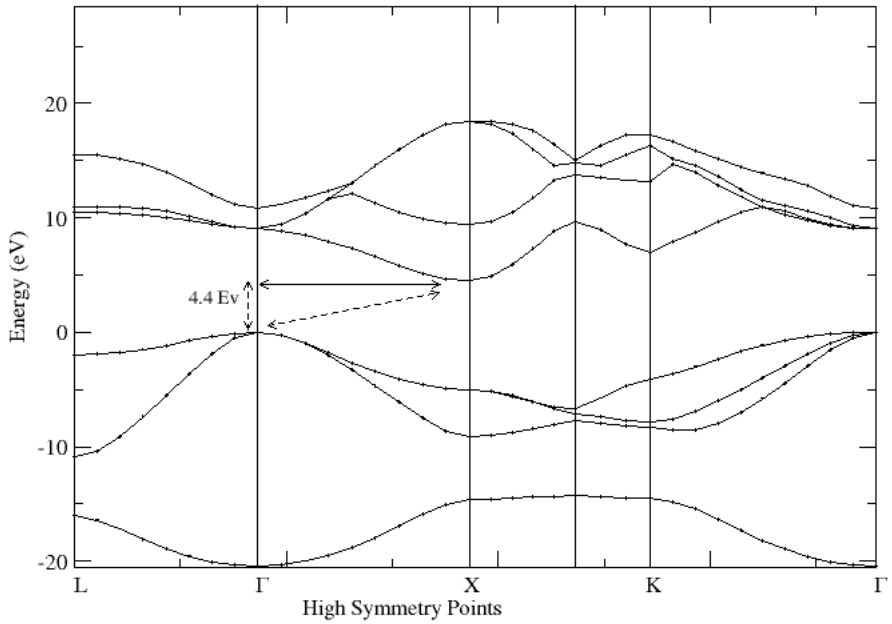

Figure 5.8: Band structure of cubic BN.

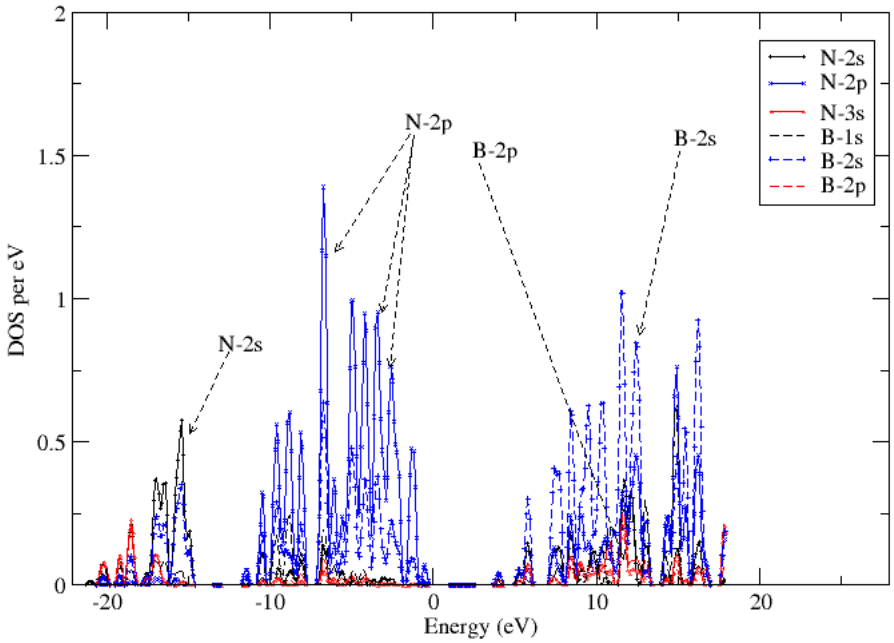

Figure 5.9: Projected Density of states for cubic BN.

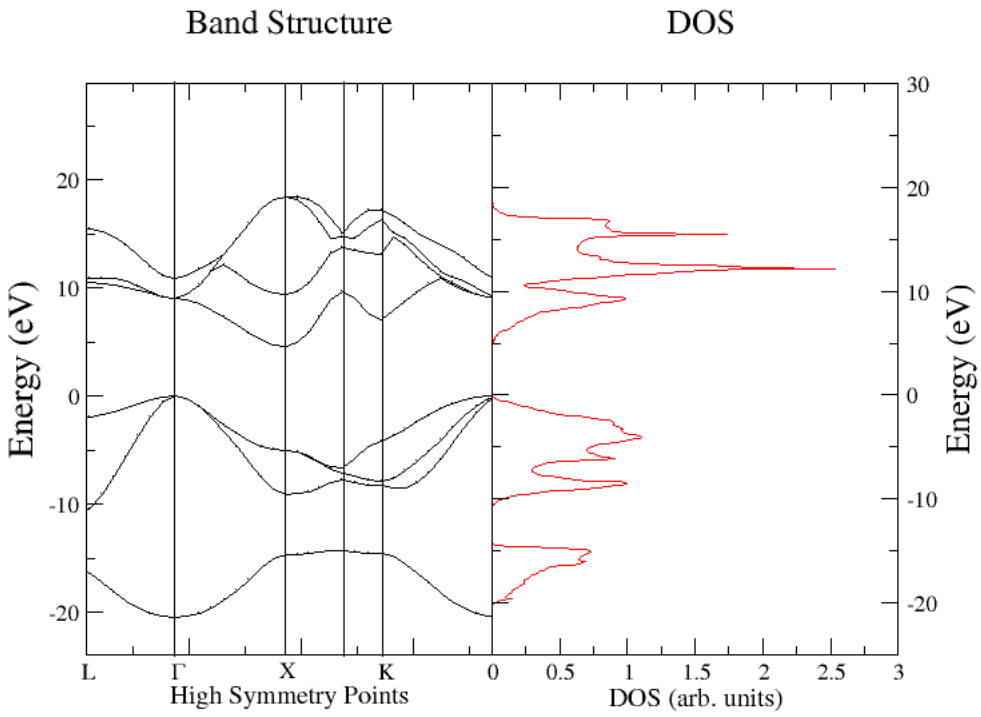

Figure 5.10: Band structure and the Density of states of cubic BN.

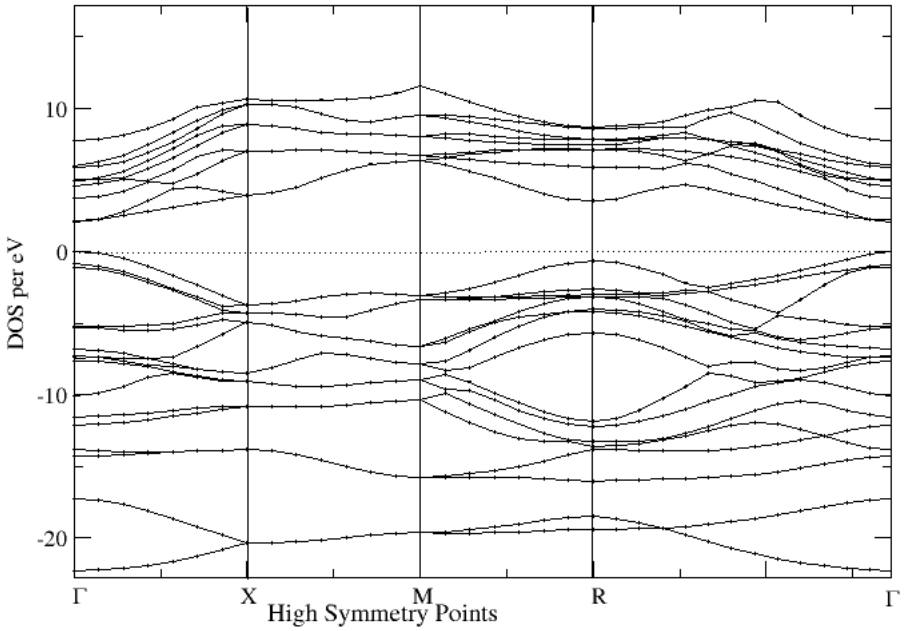

Figure 5.11: Electronic band structure of BC_2N.

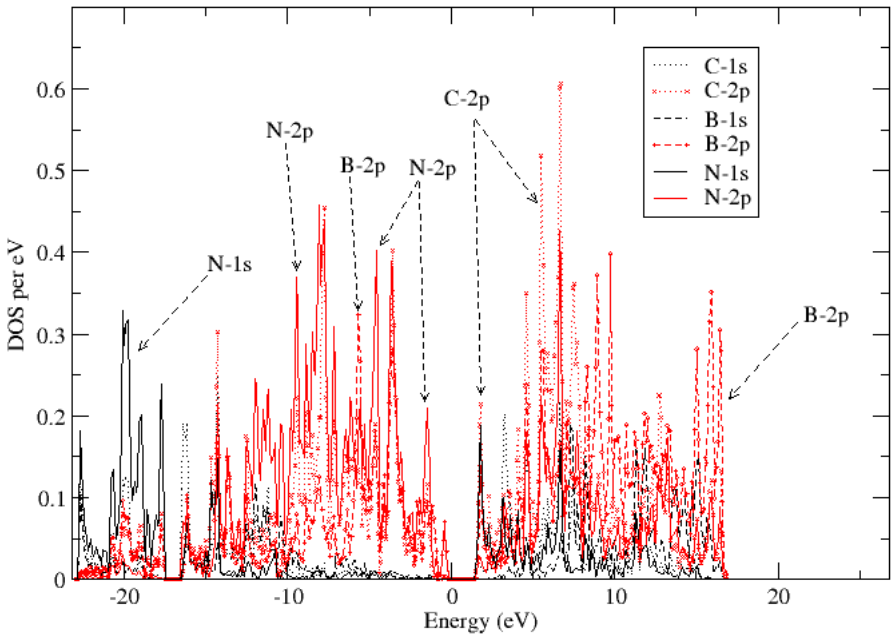

Figure 5.12: Projected density of states for BC_2N.

Figure 5.11 shows the band structure of BC_2N, while Figure 5.12 shows the corresponding density of states. The material has an easily recognizable direct band gap of 2.5 eV in its band structure. Unlike c-BN, BC_2N, has a direct band gap at Γ, with both the minima of the

conduction band and the maxima of the valence band occurring at the same point Γ. The reduction of the band gap in BC_2N is attributed to the presence of 2p orbitals of nitrogen and carbon, which contribute to the states at the valence and conduction band edges significantly (see fig 5.12).

A comparison of the band structures of c-BN and BC_2N shows that BC_2N has more bands than c-BN, and this is attributed to the added carbon atom within the matrix of BC_2N, as well as the higher number of atoms in the unit cell of BC_2N i.e 2 atoms per unit cell for c-BN and 8 atoms for BC_2N. The density of states for BC_2N shows that there is a small gap (0.7 eV) between the core states and those in the valence band, unlike the case of c-BN which has a gap between the core and valence states of about 1.9 eV. It is quite clear that both conduction and valence bands of BC_2N are wider than those of c-BN. The valence band width of BC_2N was found to be 16.6 eV, while the conduction band had a width of about 15.3 eV. On the other hand c-BN had a valence band width of about 11.34 eV, and a conduction band width of at least 15 eV. Further more, the valence band was dominated by B-2p, N-2p orbitals while the conduction band is dominated by the C-2p and B-2p orbitals. The wider valence band width as well as the presence of the C-2p, B-2p and N-2p states suggests a strong hybridization, leading to the observed high bulk modulus and hence hardness of BC_2N.

The indirect band gap of 4.4 eV suggested that c-BN was an insulator while BC_2N with its narrower bandwidth of 2.5 eV was a semiconductor. Other than their applications in the hard metal industry the small band gap of BC_2N suggests that it can be used as a semiconductor material in fast switching applications while c-BN can be used in insulating applications or in high power applications due to its wide band gap more like diamond.

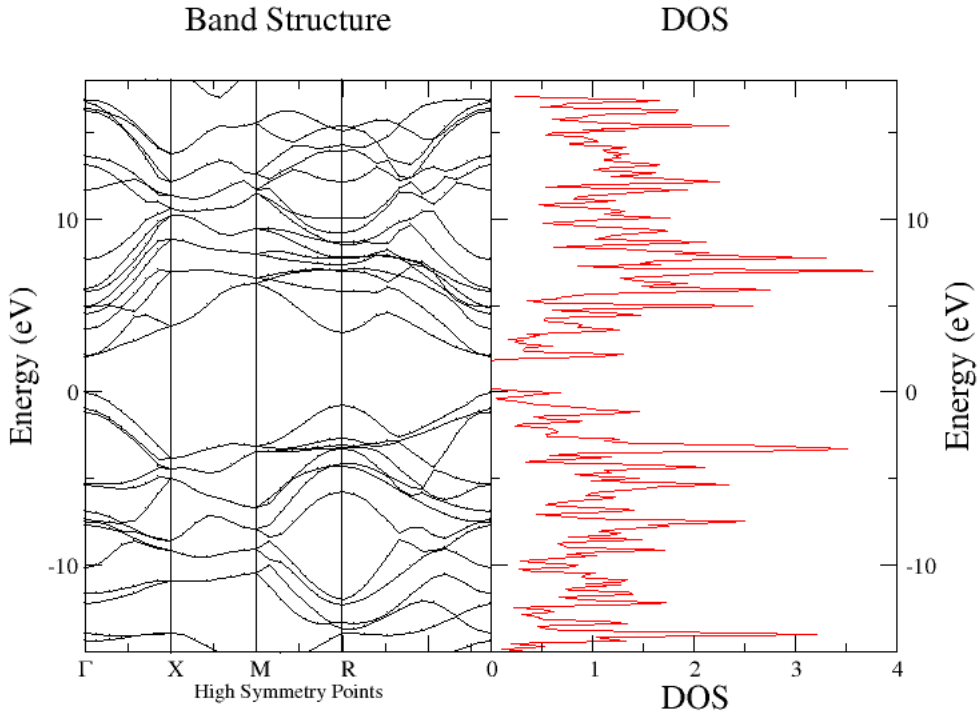

Figure 5.13: Band structure and the Density of states of BC_2N.

5.4 Vibrational and Thermodynamic Properties

The vibrational properties of any material play a big part in understanding its stability and crystal properties under different environments. As such, it was important to investigate these properties for both c-BN and BC_2N since the two materials are expected to be used in environments where both pressure and temperature change to extreme values. Figure 5.14 shows the phonon dispersion and density of states plots for c-BN, while figure 5.15 shows a similar plot for BC_2N.

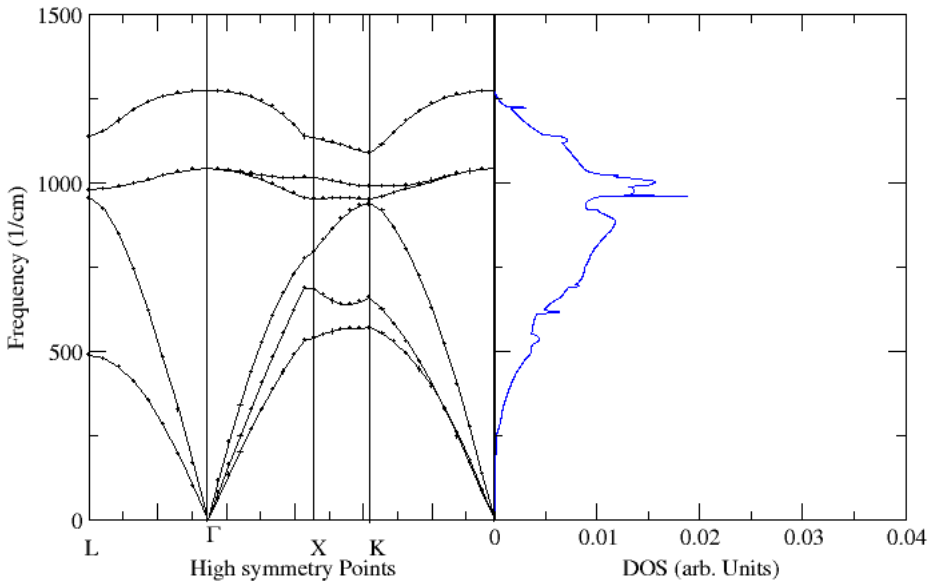

Figure 5.14: Phonon Dispersion plots and density of states for c-BN.

The phonon dispersion curves of c-BN demonstrates a small separation between the optical and the acoustic branches. There is also the splitting of the Longitudinal Optical and Transverse optical branches as well. The phonon dispersion plot of BC_2N has no separation between the optical and the acoustic branches (Figure 5.15). Fig 5.14 and 5.15 further show that the two structures demonstrated evidence of thermodynamic stability from the lack of imaginary frequencies in the phonon dispersion plots.

Fig 5.16 shows the variation of both specific heat capacity at constant volume and entropy with temperature. It is noted from the figure that it fits well to the Debye model [84].

The variation in the vibrational frequencies of c-BN with temperature as well as the internal energy is shown in figure 5.17. The same has been done for BC_2N in figures 5.18 and 5.19

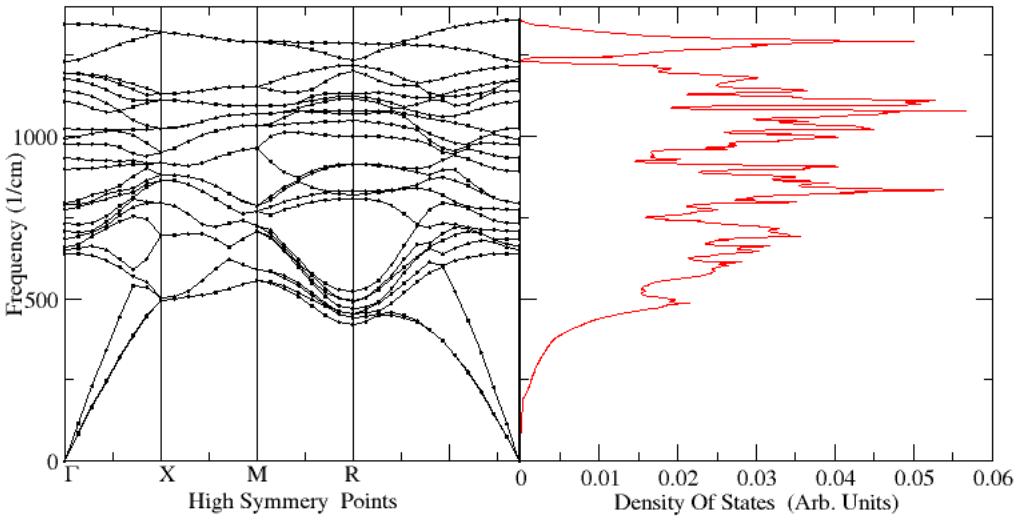

Figure 5.15: The Phonon Dispersion plots and density of states for BC_2N.

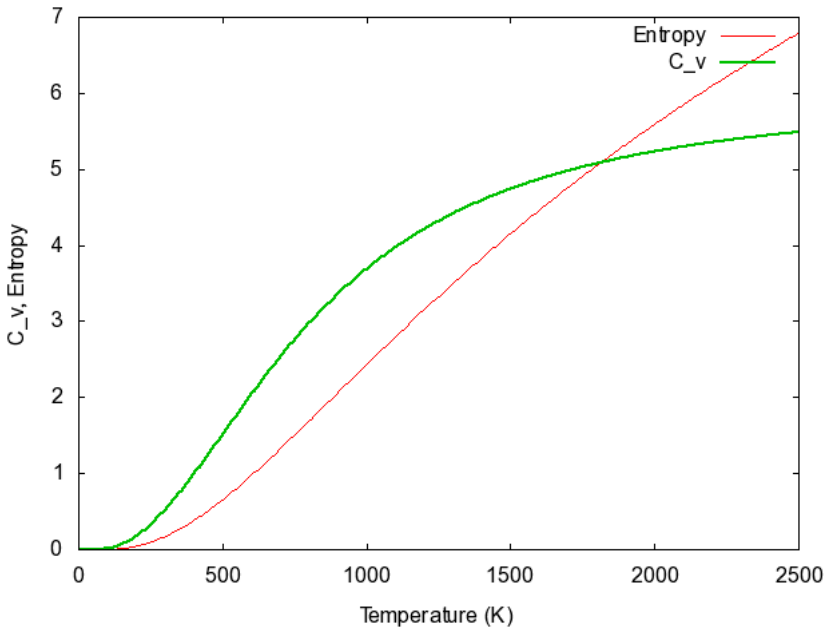

Figure 5.16: Variation in specific heat and entropy with temperature for c-BN.

for the variation of C_v and entropy with temperature, as well as internal energy and vibrational frequency with temperature, respectively. For c-BN, the entropy was observed to increase gradually with increasing temperature, while on the other hand the specific heat at constant volume increased sharply between 0-1000 K, but any increase beyond that temperature was much less pronounced, reaching a saturation value beyond 1500 K. The Internal energy on the other hand was found to grow with increasing temperature, while the vibrational frequencies decreased with increasing temperature (see figure 5.17). This behaviour was attributed to the fact that the internal energy is a function of temperature only, i.e E_{int}=$E_{int}(T)$.

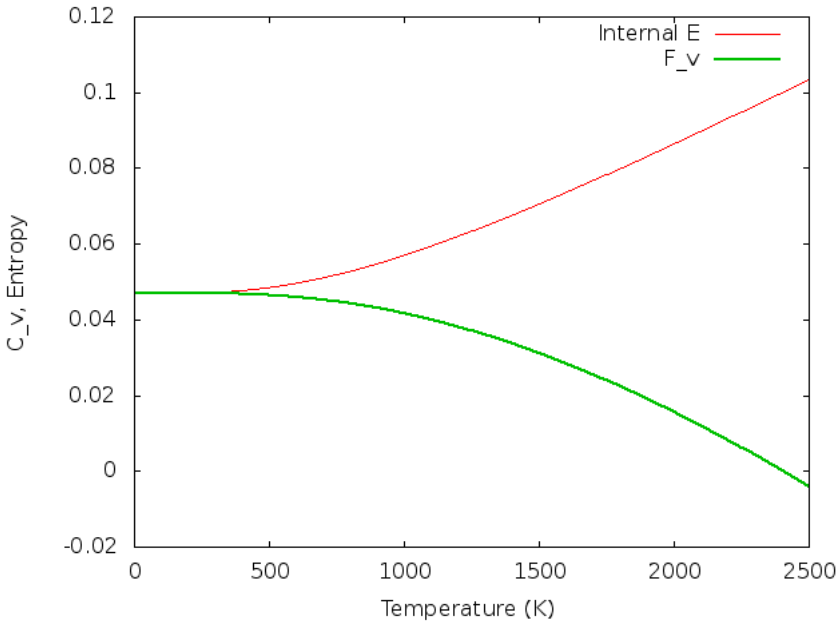

Figure 5.17: Variation in vibrational frequencies and internal energy with Temperature for c-BN.

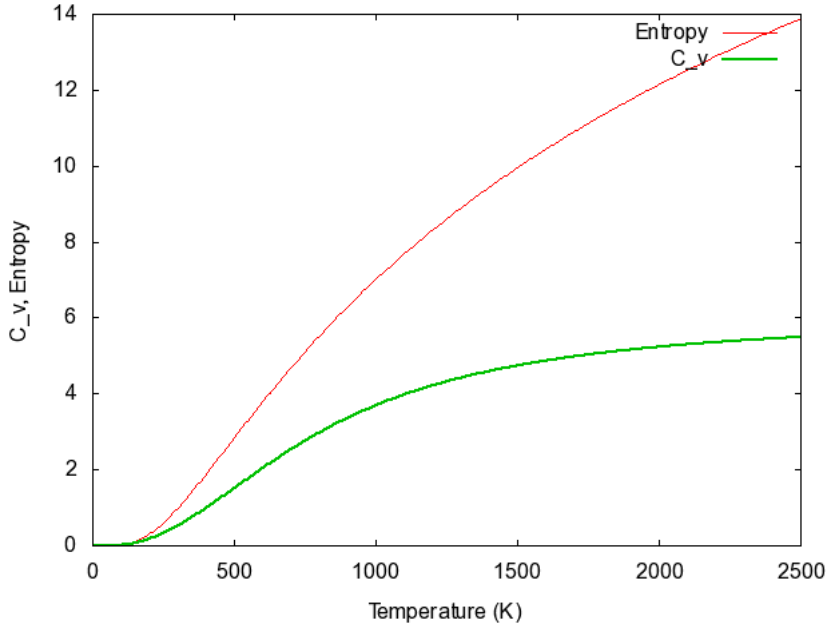

Figure 5.18: Variation in specific heat and entropy with temperature for BC_2N.

Figure 5.16 further shows that both C_v and entropy for c-BN become equal at around 1800 K, and beyond this point the entropy grew with temperature, and this growth continued well beyond 2000 K. The specific heat at constant volume on the other hand grew between 0-1000 K, but the growth from that point was much less pronounced, as it is shown in figure 5.16. In the case of BC_2N, the entropy grows much faster than the specific heat, and in fact the two never meet, unlike in the case of c-BN. C_v tends to level at about 1000 K while the entropy

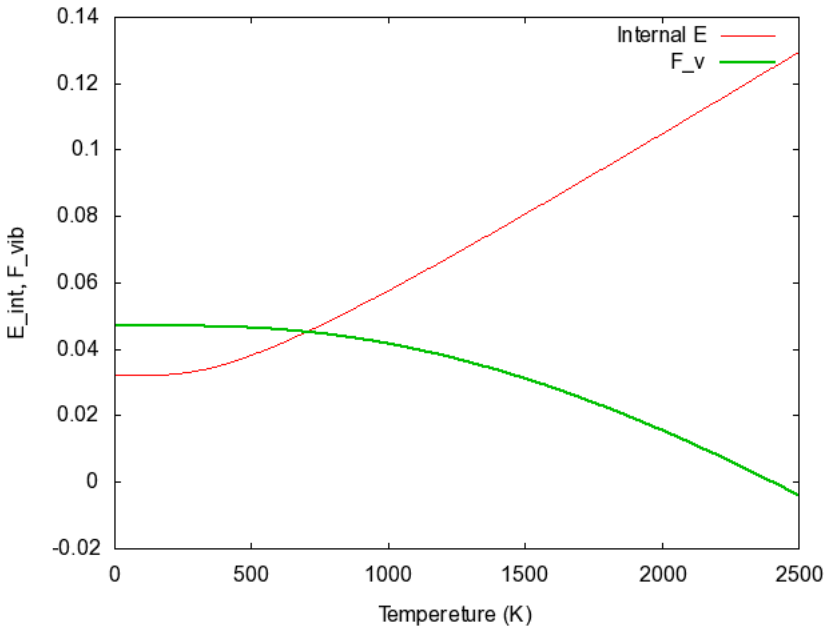

Figure 5.19: Variation in vibrational frequencies and internal energy of BC_2N with Temperature.

continues to grow with temperature, though not as fast as the range between 0-1000 K. The internal energy of BC_2N was found to start out quite low for temperatures close to 0 K but at about 700 K an inversion occurred and the internal energy grew rapidly even beyond 2000 K. In figure 5.19 the vibrational frequencies decreased from 0 K and this decrease continued as the temperature increased, due to the same reason attributed for the same behaviour in c-BN. Both Figs 5.16 and 5.18 show that the low temperature specific heat capacity C_v for c-BN and BC_2N obeyed the well known cubic law i.e. $C_v = AT^3$. The vibrational properties of both c-BN and BC_2N together with the computed elastic constants confirms that the two materials remain stable up to high temperatures which are desirable properties for materials used in harsh environments, like in drilling and machining applications, where both c-BN and BC_2N are expected to play a key role.

CHAPTER SIX

CONCLUSIONS AND RECOMMENDATIONS

6.1 Conclusions

This work has considered the lattice parameters, bulk moduli and elastic constants of BC_2N and c-BN, and it has been established that BC_2N is a superhard material due to its high bulk modulus, as well as giving evidence consistent with the material being harder than c-BN. This is confirmed by the existence of short bond lengths in BC_2N which are indicative of the strength between atoms in BC_2N compared to those in c-BN. The lattice parameter for BC_2N was found to be 3.634 Å (using DFT) and 3.613 Å (using QMC), compared to c-BN lattice parameter of 3.631 Å (using DFT) and 3.613 Å (using QMC). The bulk modulus of BC_2N was found to be 369 GPa (using DFT) and 395 GPa (from QMC), while that of c-BN was 365 GPa (using DFT) and 393 GPa (using QMC). As noted earlier, these values show good agreement with experiment, especially those from the more accurate Quantum Monte Carlo calculations.

From the electronic properties of both c-BN and BC_2N, it was found that while c-BN had a discontinuous valence band, with a very narrow conduction band, BC_2N had a continuous valence band and a fairly wider conduction band. The wide band-gap of c-BN meant that it had excellent insulating properties, while BC_2N, with the small band-gap of about 2.5 eV, was predicted to allow excitation of electrons to the conduction band at lower energies than c-BN which had a wider band gap of about 4.4 eV. The wide valence band of BC_2N showed a strong hybridization of C-2p, N-2p and B-2p orbitals, leading to the increased strength of BC_2N.

The computed elastic constants for c-BN were found to be 431 GPa (C_{44}), and 317 GPa (C'), while for BC_2N, C_{44} was found to be 457 GPa, and 360 GPa for C'. These values are consistent with the computed bulk moduli, as they are a measure of the materials response to applied stress. This therefore agrees with and supports the values of the bulk modulus that have been mentioned previously.

Also, from the results of the thermodynamic properties it was observed that the BC_2N structure was thermodynamically stable, while the calculated elastic parameters indicated mechanical stability. The findings of this study therefore confirms the stability at elevated

temperatures. The elastic parameters indicated mechanical stability of the material in relation to c-BN while the internal energy was found to depend on temperature as expected, and the computed specific heat capacity was in agreement with theory, especially the Debye law. As the temperature increased, the entropy also increased as expected, thereby predicting the correct properties of both c-BN and BC_2N.

6.2 Recommendations

Since BC_2N has demonstrated that its properties are consistent with those of a superhard material, it is recommended that further experimental work be done to better understand its properties and even synthesize it for mass production. There is also a gap in the published experimental work treating the thermodynamic and vibrational properties of BC_2N, and it is thus recommended that this gap be filled by carrying out experimental work to look at optical properties, that this study did not consider, as well as a study of the behavior of phonons in the two materials as these can also give a bearing on the hardness of the material, all these will help in validating the theoretical results that have been presented here. The commercial synthesis and application of BC_2N would be highly desirable in the future, especially in areas such as mining and related sectors that require extremely robust tools.

REFERENCES

[1] de Réaumur, R., Reaumur's Memoirs on steel and iron: a translation from the original printed in 1722. University of Chicago Press, (1956).

[2] Tian, Y., Xu, B., and Zhao, Z., "Microscopic theory of hardness and design of novel superhard crystals," International Journal of Refractory Metals and Hard Materials, (2012).

[3] Clerc, D. and Ledbetter, H., "Mechanical hardness: A semiempirical theory based on screened electrostatics and elastic shear," Journal of Physics and Chemistry of Solids, vol. 59, no. 6, pp. 1071–1095, (1998).

[4] Šimůnek, A. and Vackář, J., "Hardness of covalent and ionic crystals: First-principle calculations," Physical review letters, vol. 96, no. 8, p. 85501, (2006).

[5] Veprek, S., "The search for novel, superhard materials," Journal of Vacuum Science & Technology A: Vacuum, Surfaces, and Films, vol. 17, no. 5, pp. 2401–2420, (1999).

[6] Dubrovinskaia, N., Dubrovinsky, L., Crichton, W., Langenhorst, F., and Richter, A., "Aggregated diamond nanorods, the densest and least compressible form of carbon," Applied Physics Letters, vol. 87, no. 8, pp. 083106–083106, (2005).

[7] Zhou, W., Wu, H., and Yildirim, T., "Electronic, dynamical, and thermal properties of ultra-incompressible superhard rhenium diboride: A combined first-principles and neutron scattering study," Physical Review B, vol. 76, no. 18, p. 184113, (2007).

[8] on Superhard Materials, N. R. C. U. C., Status and applications of diamond and diamond-like materials: an emerging technology : report. Publication NMAB, National Academy Press, (1990).

[9] Grögler, T., Plewa, O., Rosiwal, S., and Singer, R., "Cvd diamond films as protective coatings on titanium alloys," International Journal of Refractory Metals and Hard Materials, vol. 16, no. 3, pp. 217–222, (1998).

[10] Novikov, N., Gontar, A., Khandozhko, S., Kutsay, A., Tkach, V., Gorokhov, V., Belitsky, G., and Vasin, A., "Protective diamond-like coatings for optical materials and electronic devices," Diamond and Related Materials, vol. 9, no. 3, pp. 792–795, (2000).

[11] Shannon, R., "Revised effective ionic radii and systematic studies of interatomic distances in halides and chalcogenides," Acta Crystallographica Section A: Crystal Physics, Diffraction, Theoretical and General Crystallography, vol. 32, no. 5, pp. 751–767, (1976).

[12] Shih, A., "An experimental investigation of rotary diamond truing and dressing of vitreous bond wheels for ceramic grinding," International Journal of Machine Tools and Manufacture, vol. 40, no. 12, pp. 1755–1774, (2000).

[13] Wentorf, Jr., R., "Cubic Form of Boron Nitride," Journal of Chemical Physics, vol. 26, p. 956, (apr 1957).

[14] Sun, H., Jhi, S., Roundy, D., Cohen, M., and Louie, S., "Structural forms of cubic BC_2N," Physical Review B, vol. 64, no. 9, p. 094108, (2001).

[15] Solozhenko, V., Dub, S., and Novikov, N., "Mechanical properties of cubic bc2n, a new superhard phase," Diamond and Related Materials, vol. 10, no. 12, pp. 2228 – 2231, (2001).

[16] Knittle, E., Kaner, R., Jeanloz, R., and Cohen, M., "High-pressure synthesis, characterization, and equation of state of cubic c-bn solid solutions," Physical Review B, vol. 51, no. 18, p. 12149, (1995).

[17] Zhuang, C., Li, X., Zhao, J., Abu Samra, H., and Jiang, X., "Fluctuations of tensile strength and hardness of c-bc2n crystals induced by difference in atomic configuration," Journal of Physics: Condensed Matter, vol. 23, p. 465401, (2011).

[18] Fan, X., Wu, H., Shen, Z., and Kuo, J., "A first-principle study on the structure, stability and hardness of cubic BC_2N," Diamond and Related Materials, vol. 18, no. 10, pp. 1278 – 1282, (2009).

[19] Zhang, Y., Sun, H., and Chen, C., "Superhard cubic BC_2N compared to diamond," Physics Review Letters, vol. 93, p. 195504, (Nov 2004).

[20] Tateyama, Y., Ogitsu, T., Kusakabe, K., Tsuneyuki, S., and Itoh, S., "Proposed synthesis

path for heterodiamond bc_2n," Physical Review B, vol. 55, no. 16, pp. 10161–10164, (1997).

[21] Solozhenko, V. and Gregoryanz, E., "Synthesis of superhard materials," Materials Today, vol. 8, no. 11, pp. 44–51, (2005).

[22] Tkachev, S., Solozhenko, V., Zinin, P., Manghnani, M., and Ming, L., "Elastic moduli of the superhard cubic bc_2n phase by brillouin scattering," Physical Review B, vol. 68, no. 5, p. 052104, (2003).

[23] Zhou, X., Sun, J., Qian, Q., Guo, X., Liu, Z., Tian, Y., and Wang, H., "A tetragonal phase of superhard bc2n," Journal of Applied Physics, vol. 105, no. 9, pp. 093521–093521, (2009).

[24] Sung, C. and Sung, M., "Carbon nitride and other speculative superhard materials," Materials chemistry and physics, vol. 43, no. 1, pp. 1–18, (1996).

[25] Korir, K., Amolo, G., Makau, N., and Joubert, D., "First-principle calculations of the bulk properties of 4d transition metal carbides and nitrides in the rocksalt, zincblende and wurtzite structures," Diamond and Related Materials, vol. 20, no. 2, pp. 157–164, (2011).

[26] Chen, X., Niu, H., Li, D., and Li, Y., "Intrinsic correlation between hardness and elasticity in polycrystalline materials and bulk metallic glasses," arXiv preprint arXiv:1102.4063, (2011).

[27] Jiang, X., Zhao, J., and Jiang, X., "Correlation between hardness and elastic moduli of the covalent crystals," Computational Materials Science, vol. 50, no. 7, pp. 2287–2290, (2011).

[28] Verma, A., "Elastic moduli and brittleness of diamondlike and zinc blende structured solids," Materials Chemistry and Physics, (2012).

[29] Yang, W., Parr, R., and Uytterhoeven, L., "New relation between hardness and compressibility of minerals," Physics and Chemistry of Minerals, vol. 15, no. 2, pp. 191–195, (1987).

[30] Goble, R. and Scott, S., "Relationship between mineral hardness and compressibility (or bulk modulus)," Canadian Mineralogist, vol. 23, no. 2, pp. 273–85, (1985).

[31] Tabor, D., "Mohs's hardness scale-a physical interpretation," Proceedings of the Physical Society. Section B, vol. 67, p. 249, (1954).

[32] Smith, R. and Sandly, G., "An accurate method of determining the hardness of metals, with particular reference to those of a high degree of hardness*," Proceedings of the Institution of Mechanical Engineers, vol. 102, no. 1, pp. 623–641, (1922).

[33] Hill, R., Storakers, B., and Zdunek, A., "A theoretical study of the brinell hardness test," Proceedings of the Royal Society of London. A. Mathematical and Physical Sciences, vol. 423, no. 1865, pp. 301–330, (1989).

[34] Oganov, A. and Lyakhov, A., "Towards the theory of hardness of materials," Journal of Superhard Materials, vol. 32, no. 3, pp. 143–147, (2010).

[35] Beckmann, G., "Über den zusammenhang zwischen kompressibilität und härte von mineralen und nichtmetallischen kristallinen substanzen," Kristall und Technik, vol. 6, no. 1, pp. 109–117, (1971).

[36] Scott, S., "Experimental calibration of the sphalerite geobarometer," Economic Geology, vol. 68, no. 4, pp. 466–474, (1973).

[37] Tse, J., "Intrinsic hardness of crystalline solids," Journal of Superhard Materials, vol. 32, no. 3, pp. 177–191, (2010).

[38] Gilman, J., Westbrook, J., and Conrad, H., "Hardnessa strength microprobe, in chapter 4 of the science of hardness testing and its research applications," American Society for Metals, Metals Park, Ohio, p. 51, (1973).

[39] Gao, F. and Gao, L., "Microscopic models of hardness," Journal of Superhard Materials, vol. 32, no. 3, pp. 148–166, (2010).

[40] Martin, R., Electronic Structure: Basic Theory and Practical Methods. Cambridge University Press, (2004).

[41] Born, M. and Oppenheimer, R., "On the quantum theory of molecules," Annalen der Physik, vol. 84, no. 20, pp. 457–484, (1927).

[42] Hartree, D., "The wave mechanics of an atom with a non-coulomb central field. part i. theory and methods," in Mathematical Proceedings of the Cambridge Philosophical Society, vol. 24, pp. 89–110, Cambridge Univ Press, (1928).

[43] Slater, J., "A simplification of the hartree-fock method," Physical Review, vol. 81, no. 3, p. 385, (1951).

[44] Slater, J. C., "The theory of complex spectra," Physical Review, vol. 34, pp. 1293–1322, (Nov 1929).

[45] Sherrill, C. D. and III, H. F. S., "The configuration interaction method: Advances in highly correlated approaches," in Advances In Quantum Chemistry (Per-Olov Lwdin, John R. Sabin, M. C. Z. and Brndas, E., eds.), vol. 34 of Advances in Quantum Chemistry, pp. 143 – 269, Academic Press, (1999).

[46] Jeziorski, B. and Monkhorst, H., "Coupled-cluster method for multideterminantal reference states," Physical Review A, vol. 24, no. 4, p. 1668, (1981).

[47] Kohn, W. and Sham, L. J., "Self-consistent equations including exchange and correlation effects," Physical Review, vol. 140, pp. A1133–A1138, (Nov 1965).

[48] Hohenberg, P. and Kohn, W., "Inhomogeneous electron gas," Physical Review, vol. 136, pp. B864–B871, (Nov 1964).

[49] Sholl, D. and Steckel, J. A., Density Functional Theory A Practical Introduction. John Wiley Sons, Inc., (April 2009).

[50] Jensen, F., Introduction to Computational Chemistry. John Wiley & Sons, (2006).

[51] Perdew, J., Burke, K., and Ernzerhof, M., "Generalized gradient approximation made simple," Physical review letters, vol. 77, no. 18, pp. 3865–3868, (1996).

[52] Perdew, J. and Wang, Y., "Accurate and simple analytic representation of the electron-gas correlation energy," Physical Review B, vol. 45, no. 23, p. 13244, (1992).

[53] Perdew, J., Burke, K., and Wang, Y., "Generalized gradient approximation for the exchange-correlation hole of a many-electron system," Physical Review B, vol. 54, no. 23, p. 16533, (1996).

[54] Zhang, Y. and Yang, W., "A challenge for density functionals: Self-interaction error increases for systems with a noninteger number of electrons," The Journal of chemical physics, vol. 109, no. 7, pp. 2604–2608, (1998).

[55] Baroni, S., Giannozzi, P., and Isaev, E., "Thermal properties of materials from ab-initio quasi-harmonic phonons," arXiv preprint arXiv:1112.4977, (2011).

[56] Foulkes, W., Mitas, L., Needs, R., and Rajagopal, G., "Quantum monte carlo simulations of solids," Reviews of Modern Physics, vol. 73, no. 1, p. 33, (2001).

[57] Richard Needs, Mike Towler, N. D. and Rios, P. L., "Casino version 2.5.0 users manual," University of Cambridge, Cambridge, (2000).

[58] Dewing, M., "Improved efficiency with variational monte carlo using two level sampling," The Journal of Chemical Physics, vol. 113, no. 13, pp. 5123–5125, (2000).

[59] Alfè, D. and Gillan, M., "Efficient localized basis set for quantum monte carlo calculations on condensed matter," Physical Review B, vol. 70, no. 16, p. 161101, (2004).

[60] Giannozzi, P., Baroni, S., Bonini, N., Calandra, M., Car, R., Cavazzoni, C., Ceresoli, D., Chiarotti, G., Cococcioni, M., Dabo, I., and others,, "Quantum espresso: a modular and open-source software project for quantum simulations of materials," Journal of Physics Condensed Matter, vol. 21, p. 5502, (Sept. 2009).

[61] Needs, R., Towler, M., Drummond, N., and Ríos, P., "Continuum variational and diffusion quantum monte carlo calculations," Journal of Physics Condensed Matter, vol. 22, p. 023201, (jan 2010).

[62] "Gnu general public license, version 3." `http://www.gnu.org/licenses/gpl.html`, (June 2007). Last retrieved 2012-05-10.

[63] Johnson, D., "Modified broydens method for accelerating convergence in self-consistent calculations," Physical Review B, vol. 38, no. 18, p. 12807, (1988).

[64] Hamann, D., Schlüter, M., and Chiang, C., "Norm-conserving pseudopotentials," Physical Review Letters, vol. 43, no. 20, pp. 1494–1497, (1979).

[65] Kresse, G. and Joubert, D., "From ultrasoft pseudopotentials to the projector augmented-wave method," Physical Review B, vol. 59, no. 3, p. 1758, (1999).

[66] Giannozzi, P., De Angelis, F., and Car, R., "First-principle molecular dynamics with ultrasoft pseudopotentials: parallel implementation and application to extended bio-inorganic system," arXiv preprint cond-mat/0311507, (2003).

[67] Blöchl, P., "Projector augmented-wave method," Physical Review B, vol. 50, no. 24, p. 17953, (1994).

[68] Fletcher, R., Practical methods of optimization, Volume 1. Wiley, (1987).

[69] Billeter, S., Turner, A., and Thiel, W., "Linear scaling geometry optimisation and transition state search in hybrid delocalised internal coordinates," Phys. Chem. Chem. Phys., vol. 2, no. 10, pp. 2177–2186, (2000).

[70] Billeter, S., Curioni, A., and Andreoni, W., "Efficient linear scaling geometry optimization and transition-state search for direct wavefunction optimization schemes in density functional theory using a plane-wave basis," Computational materials science, vol. 27, no. 4, pp. 437–445, (2003).

[71] Monkhorst, H. and Pack, J., "Special points for brillouin-zone integrations," Physical Review B, vol. 13, no. 12, pp. 5188–5192, (1976).

[72] Soma, T., Sawaoka, A., and Saito, S., "Characterization of wurtzite type boron nitride synthesized by shock compression," Materials Research Bulletin, vol. 9, no. 6, pp. 755–762, (1974).

[73] Mehl, M., Klein, B., and Papaconstantopoulos, D., "First-principles calculations of elastic properties of metals," Intermetalic Compounds: Principles and Practice, vol. 1, (1994).

[74] Clerc, D., "Ab initio elastic properties of diamond-like materials: electronic factors that determine a high bulk modulus," Journal of Physics and Chemistry of Solids, vol. 60, no. 1, pp. 103–110, (1999).

[75] Solozhenko, V., Andrault, D., Fiquet, G., Mezouar, M., and Rubie, D., "Synthesis of superhard cubic bcn," Applied Physics Letters, vol. 78, p. 1385, (2001).

[76] Nakano, S., Akaishi, M., Sasaki, T., and Yamaoka, S., "Segregative crystallization of several diamond-like phases from the graphitic bc2n without an additive at 7.7 gpa," Chemistry of materials, vol. 6, no. 12, pp. 2246–2251, (1994).

[77] Andrievskiy, R., "New superhard nanomaterials-based high-melting point compounds," TiC, vol. 30, no. 2, p. 288, (2007).

[78] Solozhenko, V., "In situ studies of high-pressure phase transformations in the b–c–n system," High Pressure Research, vol. 24, no. 4, pp. 499–509, (2004).

[79] Grimsditch, M., Zouboulis, E., and Polian, A., "Elastic constants of boron nitride," Journal of applied physics, vol. 76, no. 2, pp. 832–834, (1994).

[80] Rodriguez-Hernandez, P., Gonzalez-Diaz, M., and Munoz, A., "Electronic and structural properties of cubic bn and bp," Physical Review B, vol. 51, no. 20, p. 14705, (1995).

[81] Kim, K., Lambrecht, W., and Segall, B., "Erratum: Elastic constants and related properties of tetrahedrally bonded bn, aln, gan, and inn," Physical Review B, vol. 56, no. 11, pp. 7018–7018, (1997).

[82] Xu, Y.-N. and Ching, W. Y., "Calculation of ground-state and optical properties of boron nitrides in the hexagonal, cubic, and wurtzite structures," Phys. Rev. B, vol. 44, pp. 7787–7798, (Oct 1991).

[83] Watanabe, M., Itoh, S., Sasaki, T., and Mizushima, K., "Visible-light-emitting layered BC_2N semiconductor," Physical review letters, vol. 77, no. 1, pp. 187–189, (1996).

[84] Razeghi, M., Fundamentals of Solid State Engineering. Springer London, Limited, (2009).

APPENDIX A

OPTIMIZATION

A.1 Structural Optimization

The structural representation of the unit cell of both c-BN and BC_2N were optimized to be able to get an accurate model of the ground state of the two materials. This procedure involved optimizing the size of the Monkhorst-Pack grid, the plane wave cut-off energy as mentioned before, and finally the lattice parameter of the crystal.

A.1.1 K-Point Optimization

An optimal size of the Monkhorst Pack scheme of k-points was selected, with the accuracy and the computational tractability being the guiding factors in the choice. A mesh size of $4 \times 4 \times 4$ was selected for c-BN and $3 \times 3 \times 3$ for the BC_2N system. This maintained the accuracy of the ensuing calculations, as well as making sure that the calculations would be feasible on a practical time scale.

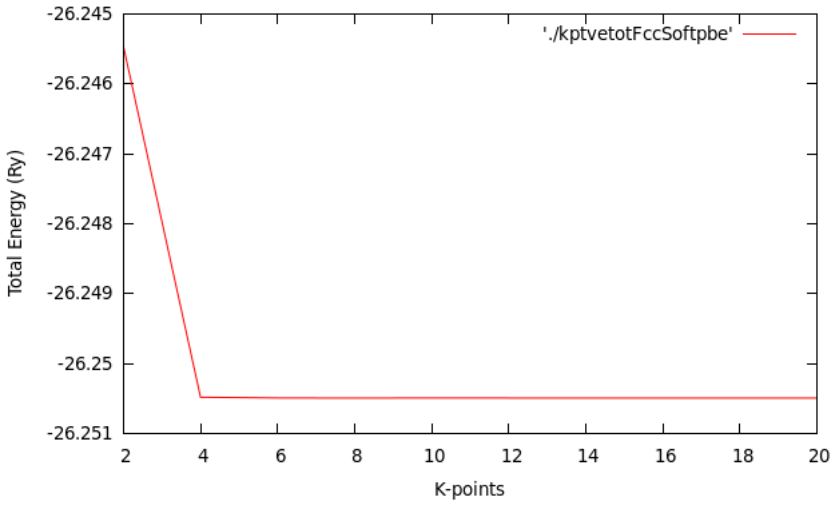

Figure A.1: Results for k-point optimization for cubic boron Nitride.

Figure A.1 shows the behaviour of the energy of the system as a function of the size of the the mesh, while figure A.2 shows the same for the BC_2N structure. There is clear convergence for the energy in the c-BN structure from the $4 \times 4 \times 4$ size, for reasons of computational tractability, the mesh size for BC_2N was restricted to $3 \times 3 \times 3$.

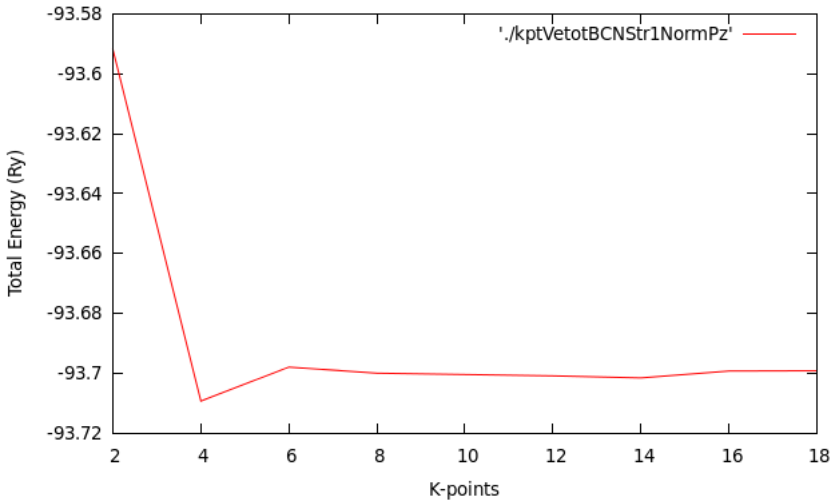

Figure A.2: Results for k-point optimization for carbon boron Nitride.

A.1.2 Plane Wave Energy Cut-off

The plane wave cut-off energy (E-cut) was optimized after the k-point optimization. This led to an optimized value of $70Ry$ being chosen for the BC_2N system, and a value of $90Ry$ for the c-BN system. The behaviour of plane wave cut-off energy with total energy is shown in figure A.3 for c-BN, and in figure A.4 for BC_2N.

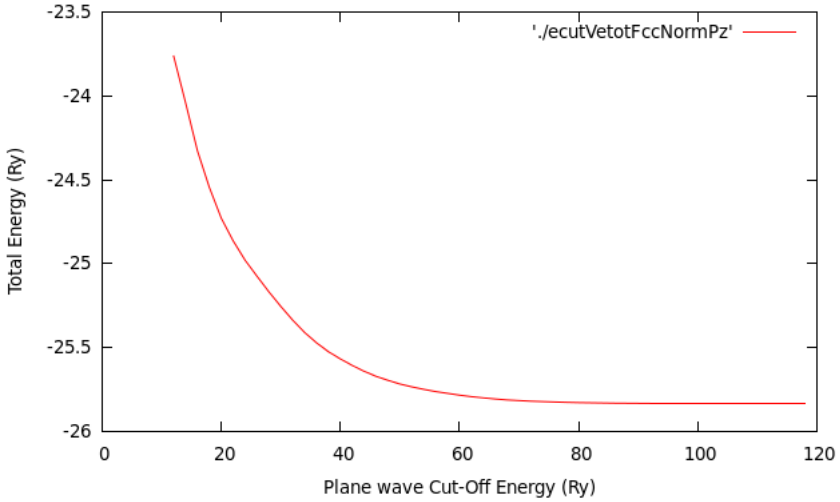

Figure A.3: Plane wave cut-off optimization for boron Nitride.

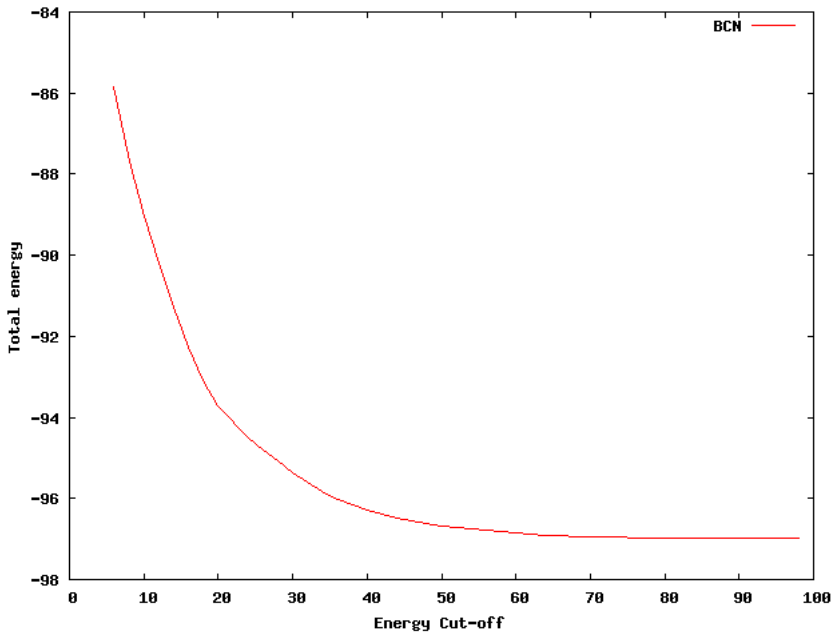

Figure A.4: Plane wave cut-off optimization for carbon boron Nitride.

These values of the plane wave cut-off energy were high since norm-conserving pseudo potentials were used, and these generally lead to higher cut-off energies.

A.1.3 Lattice Parameter Optimization

The lattice parameter was also optimized to find the equilibrium value of the parameter in the ground state for the two materials. The behaviour of the total energy of the structures with lattice parameter is shown in figure A.5 for c-BN and figure A.6 for BC_2N.

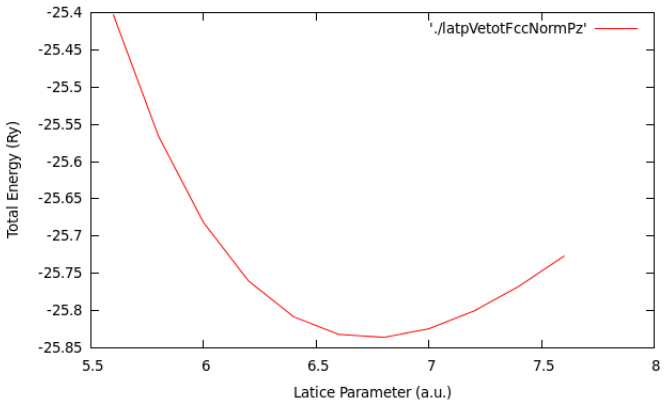

Figure A.5: Energy as a function of the lattice parameter for c-BN.

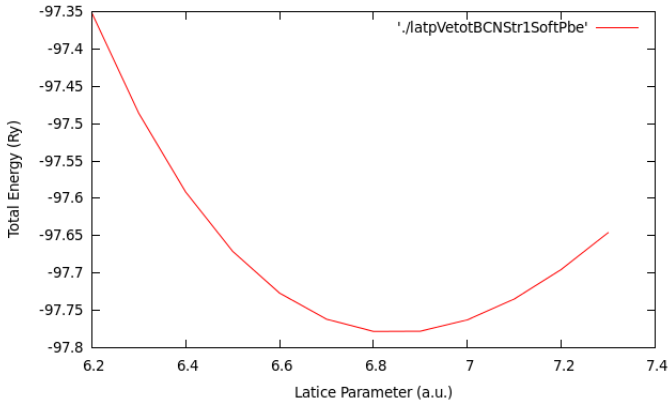

Figure A.6: Energy as a function of the lattice parameter for BC_2N.

A.1.4 Equilibration Characteristics of c-BN and BC_2N

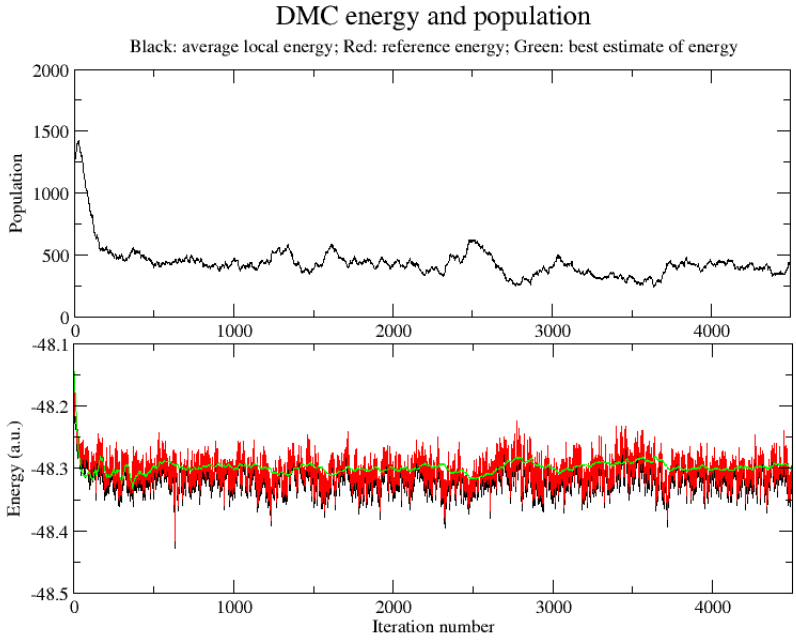

Figure A.7: Equilibration characteristics for c-BN. Upper panel represents the population size against the iteration number, while the lower panel represents the energy change as a function of the iteration number.

Presented in figures A.7 and A.8 is the equilibration of the energy with iterations during the DMC step. These figures show the behaviour of the energy of the systems as the system evolved in time. The convergence towards an average value after some initial equilibration is demonstrated.

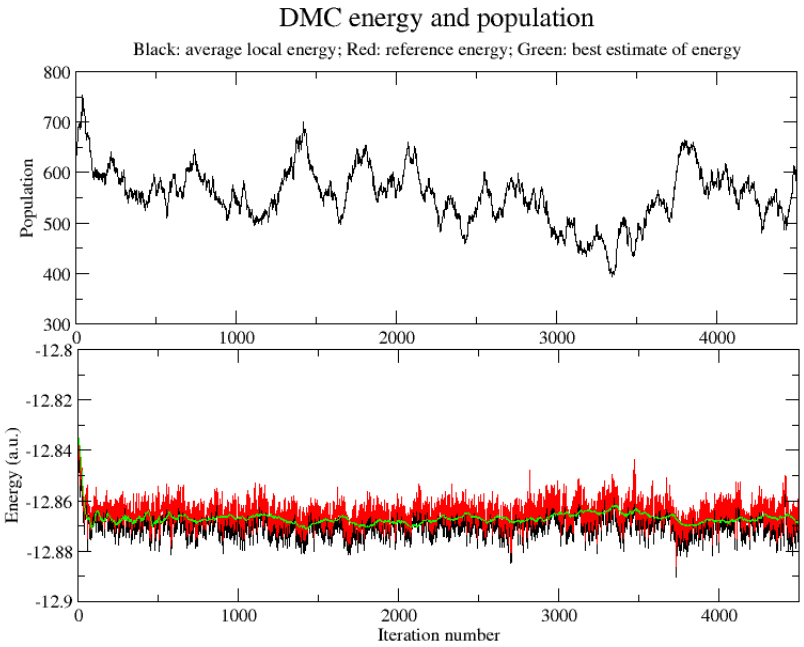

Figure A.8: Equilibration characteristics for BC_2N. Upper panel represents the population size against the iteration number, while the lower panel represents the energy change as a function of the iteration number.

APPENDIX B

CONFERENCE PRESENTATIONS, SCHOOLS AND WORKSHOPS ATTENDED

B.1 Conference Presentations

1. M.O. Atambo, G. O. Amolo, N. W. Makau, Mechanical and electronic properties of cubic BN and BC_2N, "First national science, technology and innovation week", KICC, $7^{th} - 11^{th}$ May 2012. **Awarded 2^{nd} place in Best scientific Presentations**.

2. M.O. Atambo, G. O. Amolo, N. W. Makau, First Principle Calculation of Mechanical and Electronic Properties of BN and BC_2N, Inaugural conference of nanotechnology and material science development in Kenya, Kenyatta University, Juja, $18^{th} - 20^{th}$ July 2012.

B.2 Schools and Workshops Attended

1. African School on Electronic Structure Methods and Applications (ASESMA -2012), Chepkoilel University College, Eldoret, Kenya, 28^{th} May to 8^{th} June 2012.

2. 16th International Workshop on Computational Physics and Materials Science: Total Energy and Force Methods, the I.C.T.P. Miramare -Trieste, Italy, $10 - 12^{th}$ January 2013.

3. Hands-on Tutorial on Electronic Structure computations, the I.C.T.P, Miramare-Trieste, Italy, $14 - 18^{th}$ January 2013.

4. JAIST International Winter school 2012: Quantum Monte Carlo Electronic Structure Calculation, Japan Advance Inst. of Sci. and Tech, Ishikawa, Japan, $19 - 23^{rd}$ February 2013.